Density Functional Study of the In-Line Mechanism of Methanolysis of Cyclic Phosphate and Thiophosphate Esters in Solution: Insight into Thio Effects in RNA Transesterification

Yun Liu,[†] Brent A. Gregersen,[†] Xabier Lopez,[‡] and Darrin M. York*[,†]

Department of Chemistry, University of Minnesota, 207 Pleasant St. SE, Minneapolis, Minnesota 55455-0431, and Kimika Fakultatea, Euskal Herriko Unibertsitatea, P. K. 1072, 20080 Donostia, Euskadi, Spain

Received: June 10, 2005; In Final Form: August 30, 2005

Density functional calculations of thio effects on the in-line mechanism of methanolysis of ethylene phosphate (a reverse reaction model for RNA phosphate transesterification) are presented. A total of 12 reaction mechanisms are examined using the B3LYP functional with large basis sets, and the effects of solvation were treated using the PCM, CPCM, and SM5 solvation models. Single thio substitutions at all of the distinct phosphoryl oxygen positions (2′, 3′, 5′, pro-R) and a double thio substitution at the nonbridging (pro-R/pro-S) positions were considered. Profiles for each reaction were calculated in the dianionic and monoanionic/monoprotic states, corresponding to reaction models under alkaline and nonalkaline conditions, respectively. These models provide insight into the mechanisms of RNA transesterification thio effects and serve as a set of high-level quantum data that can be used in the design of new semiempirical quantum models for hybrid quantum mechanical/molecular mechanical simulations and linear-scaling electronic structure calculations.

1. Introduction

That RNA can act as an enzyme (ribozyme) to catalyze complex biological reactions, including the transphosphorylation and hydrolysis of phosphodiester bonds, has generated great interest in the study of the underlying catalytic mechanisms. The elucidation of the molecular mechanism of RNA catalysis is immensely important for the design of medical therapies that target genetic disorders[1−3] as well as the development of new biotechnology.[4−8]

A variety of experimental methods have been used to study the cleavage of phosphodiester bonds by ribozymes[9−13] as well as the nonenzymatic pathways for the transphosphorylation and hydrolysis of RNA and related model phosphate systems in solution.[14−16] Of particular relevance to the present study is the cleavage transesterification reaction (Scheme 1) that occurs in RNA and is catalyzed by the prototype RNA enzymes such as the hammerhead[17,18] and hairpin[19,20] ribozymes. One method to probe the mechanism of ribozymes is to introduce chemical modifications at specific sites[6,21−25] and make mechanistic inferences from the measured change in reaction rate. A commonly applied modification involves the substitution of key phosphoryl oxygens with sulfur.[15,21,23,25,26] A subsequent change in the reaction rate is called a *thio effect*, and can provide insight into the specific role these positions play in the biological reaction. However, it is often the case that multiple mechanistic pathways are able to fit the observed kinetics equally well.[27] Theoretical methods offer a potentially powerful tool to aid in the mechanistic interpretation of experimental kinetic data and provide additional atomic-level insight into the structural and chemical reaction dynamics.[28−31]

Quantum electronic structure methods offer a means to study chemical reactions of biological phosphates. These systems have been the focus of theoretical studies in the gas phase,[32−36] in solution,[3−45] (including ab initio studies of the nature of associative and dissociative paths[46−48]), and in enzymatic environments.[49−51] Relatively few electronic structure studies, however, have addressed the issue of the effect of sulfur substitution on biological phosphate systems,[52−55] and only a handful have directly studied thio effects on the in-line attack mechanism.[53,56,57]

In the present work, density functional methods are used to study the in-line mechanism of methanolysis of ethylene phosphate (a reverse reaction model for RNA phosphate transesterification) and a series of single and double thiosubstituted analogues. For each model system, both dianionic and monoanionic reaction models are presented. These models provide insight into the mechanisms of RNA transesterification thio effects under alkaline and nonalkaline conditions and serve as a set of high-level quantum data that can be used in the design of new semiempirical quantum models for hybrid quantum mechanical/molecular mechanical simulations and linear-scaling electronic structure calculations.

2. Methods

2.1. Density Functional Calculations. The present work presents density functional electronic structure calculations for thio effects on the in-line mechanism of methanolysis of ethylene phosphate, the reverse reaction being a model for RNA transesterification (Scheme 1). Mechanisms for both dianionic (Scheme 2) and monoanionic/monoprotic (Scheme 3) systems were considered. Calculations were performed using Kohn−Sham density functional theory (DFT) with the hybrid exchange functional of Becke[58,59] and the Lee, Yang, and Parr correlation functional[60] (B3LYP). Energy minimum and transition state geometry optimizations were carried out in redundant internal coordinates with default convergence criteria,[61] while the stability conditions of the restricted closed-shell Kohn−Sham determinant for each final structure were verified.[62,63] Frequency

* Corresponding author. E-mail: York@chem.umn.edu.
[†] Department of Chemistry, University of Minnesota.
[‡] Kimika Fakultatea, Euskal Herriko Unibertsitatea.

10.1021/jp053146z CCC: $30.25
Published on Web 10/04/2005

SCHEME 1: RNA Transesterication

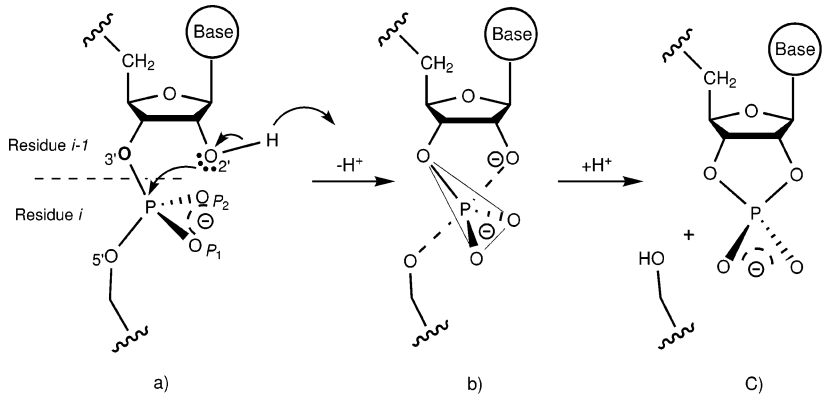

SCHEME 2: In-Line Dianionic Mechanism of Ethylene Phosphate Methanolysis (a Reverse-Reaction Model for RNA Phosphate Transesterication)

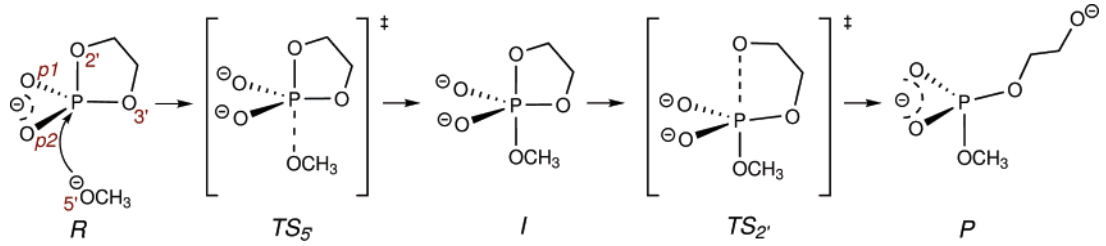

SCHEME 3: In-Line Monoanionic Mechanism of Ethylene Phosphate Methanolysis (a Reverse-Reaction Model for RNA Phosphate Transesterication)

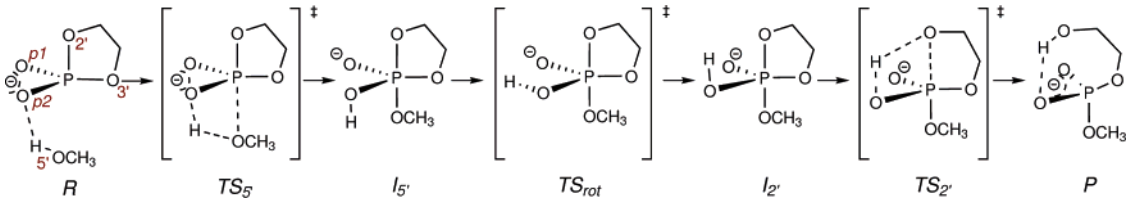

calculations were performed to establish the nature of all stationary points and to allow evaluation of thermodynamic quantities.

Geometry optimization and frequency calculations were performed using the 6-31++G(d,p) basis set. Electronic energies were further refined via single point calculations at the optimized geometries using the 6-311++G(3df,2p) basis set and the B3LYP hybrid density functional.

All single point calculations were run with convergence criteria on the SCF wave function tightened to 10^{-8} *au* to ensure high precision for properties sensitive to the use of diffuse basis functions.[64] The protocol applied to obtain the (refined energy)// (geometry and frequencies) is designated by the abbreviated notation B3LYP/6-311++G(3df,2p)//B3LYP/6-31++G(d,p). All density functional calculations were performed with the GAUSSIAN03[65] suite of programs (with the exception of the SM5 solvation calculations, see below). This density functional protocol has been extensively tested and applied to biological phosphate systems.[54,55,66−68] Thermodynamic properties at 298.15 K were obtained from the density functional calculations by using standard statistical mechanical expressions for separable vibrational, rotational, and translational contributions within the harmonic oscillator, rigid rotor, ideal gas/particle-in-a-box models in the canonical ensemble[69] and have been described in detail elsewhere.[66] The standard state in the gas phase was for a mole of particles at 1 atm pressure, and in solution was 1 M concentration.

2.2. Solvation Models. Solvent effects were examined using additional single point calculations at the gas-phase-optimized B3LYP/6-31++G(d,p) geometries as in previous work.[54,55,66−68] Three different solvation models[70] were considered for comparison: (1) the polarizable continuum model (PCM),[71−73] (2) a variation of the conductor-like screening model (COSMO)[74] (employing the parameters provided by Klamt and coworkers[75]) as implemented in GAUSSIAN03,[65,76] and (3) the SM5.42R solvation model (SM5)[77] as implemented in MNGSM.[78]

The solvation free energy, ΔG_{sol}, is defined as

$$\Delta G_{sol} = G_{aq} - G_{gas} \quad (1)$$

where G_{gas} and G_{aq} are the molecular free energies in the gas phase and in aqueous solution, respectively. In the present work, the approximation was made that the gas-phase geometry, entropy, and thermal corrections to the enthalpy do not change upon solvation. This approximation is consistent with that of recent work on related systems,[54,55,66−68] where the protocol was tested against the most relevant available experimental values and found to be generally reliable for the models considered. The practical reason for using gas-phase-optimized structures (i.e., neglecting solvent-induced structural relaxation) resides in the discontinuous gradients and computational cost associated with the calculation of stationary points and Hessians with some boundary element solvation methods. Methods that help alleviate this problem have been introduced[79] and recently been integrated with electronic structure methods at the semiempirical level[80] and are beginning to realize application.[81]

Within these approximations, the solvation energy is given by

$$\Delta G_{sol} = (E[\Psi_{sol}] + E_{sol}[\rho_{sol}]) - E[\Psi_{gas}] \qquad (2)$$

where $E[\Psi_{gas}]$ and $E[\Psi_{sol}]$ are the Kohn−Sham energy functionals that take as arguments the Kohn−Sham single-determinant wave function optimized in the gas phase (Ψ_{gas}) and in solution (Ψ_{sol}), and $E_{sol}[\rho_{sol}]$ is the solvation energy that takes as argument the polarized electron density in solution ρ_{sol} (which can be derived from Ψ_{sol}).

All PCM and COSMO single point calculations were performed at the B3LYP/6-311++G(3df,2p) level with the optimized gas-phase geometries using the UAKS radii.[82] All SM5.42R calculations were carried out using the B3LYP functional and the MIDI! basis set[83] at the optimized gas-phase geometries. The SM5.42R/B3LYP/MIDI! model was parametrized using HF/MIDI! derived geometries; however, the original SM5.42R model is relatively insensitive to small changes in geometry.[77] Additional details on the application of this method to related systems is discussed elsewhere.[66]

3. Results

3.1. Dianionic Reactions. Scheme 2 illustrates the general mechanism for dianionic in-line methanolysis of ethylene phosphate with phosphoryl oxygen positions labeled in accord with their RNA counterparts involved in RNA transesterification (Scheme 1).

3.1.1. Structure and Mechanism. The key structural parameters for stationary points along the dianionic reaction mechanisms are listed in Table 1. The unsubstituted substrate is ethylene phosphate, a cyclic phosphate with a phosphodiester P−O bond length of 1.709 Å and an endocyclic P−O−C bond angle of 110.8°. This implies a slightly elongated phosphodiester P−O bond length by around 0.027 Å with respect to dimethyl phosphate, an acyclic analogue, and a strained (contracted) endocyclic P−O−C bond angle by around 7° relative to dimethyl phosphate.

The native dianionic reaction proceeds through a single early $TS_{5'}$-type transition state with an elongated P−$O_{5'}$ bond (2.453 Å) and a considerably distorted trigonal bipyramidal structure (θ_{ax} = 163.2°). The product structure is an acyclic phosphate diester with the 2′ alkoxide leaving group extended (P−$O_{2'}$ distance greater than 5 Å) and forming a right angle with the 5′ nucleophile ($O_{5'}$−P−$O_{2'}$ angle of 90°). The (−O−CH_2−CH_2−$O_{2'}$−) chain of the product structure is in a *trans* conformation around the C−C single bond. Sulfur substitution at the nonbridging phosphoryl oxygen positions (O_{P1} and O_{P2}) results in an earlier $TS_{5'}$ transition state with less associative character: the P−$O_{5'}$ bond length increases from 2.453 Å in the native reaction to 2.655 and 2.823 Å in the singly (S:O_{P1}) and doubly (S:O_{P1},O_{P2}) substituted reactions, respectively.

A striking feature of the dianionic reactions with sulfur substitution(s) at the nonbridging position is the appearance of a stable phosphorane intermediate and a late $TS_{2'}$-type transition state (which is not rate limiting). The intermediate I is slightly more in-line with θ_{ax} angles of 166.3° and 168.1°, respectively. The $TS_{2'}$ transition state is slightly less distorted in terms of the θ_{ax} angle than the $TS_{5'}$ transition states. The $TS_{2'}$ becomes a later transition state with increased sulfur substitution (longer P−$O_{2'}$ bond lengths) at the nonbridging positions, analogous to the lengthening of the P−$O_{5'}$ bonds with increased sulfur substitution in the $TS_{5'}$ transition state.

TABLE 1: Structural Characterization of Stationary Points for Native and Thiosubstituted In-Line Dianionic Mechanism of Ethylene Phosphate Methanolysis in the Gas Phase[a]

	dianionic			
reaction	structure	$r(P-X_{5'})$	$r(P-X_{2'})$	θ_{ax}
native	R		1.709	
	$TS_{5'}$	2.453	1.841	163.2
	I			
	$TS_{2'}$			
	P	1.700	5.136	90.0
S:O_{P1}	R		1.703	
	$TS_{5'}$	2.655	1.781	161.5
	I	1.815	1.945	166.3
	$TS_{2'}$	1.779	2.223	166.3
	P	1.693	5.105	89.6
S:O_{P1},O_{P2}	R		1.703	
	$TS_{5'}$	2.823	1.767	160.0
	I	1.786	1.888	168.1
	$TS_{2'}$	1.739	2.405	165.7
	P	1.685	5.127	86.6
S:$O_{3'}$	R		1.691	
	$TS_{5'}$	2.329	1.815	157.0
	I			
	$TS_{2'}$			
	P	1.694	5.658	84.6
S:$O_{5'}$	R		1.709	
	$TS_{5'}$			
	I			
	$TS_{2'}$	2.537	2.513	166.7
	P	2.237	5.128	98.5
S:$O_{2'}$	R		2.244	
	$TS_{5'}$	2.757	2.538	161.1
	I			
	$TS_{2'}$			
	P	1.703	5.546	88.8

[a] Distance quantities (r) are in Å, and angular quantities (θ) are in degrees. The angular quantity θ_{ax} is the axial $X_{5'}-P-X_{2'}$ angle.

Sulfur substitution at the 3′ position (S:$O_{3'}$) slightly increases the associative character of $TS_{5'}$ with a P−$O_{5'}$ bond length of 2.329 Å. The 3′ sulfur in the equatorial position increases the effective repulsions with the axial ligands around phosphorus and leads to a distortion of the trigonal bipyramidal structure of $TS_{5'}$ (θ_{ax} = 157.0°) by 6.2° relative to the native reaction, but otherwise has a minor effect on the mechanism.

Sulfur substitution at the nucleophilic 5′ position (S:$O_{5'}$) has a dramatic effect on the mechanism and leads to a single $TS_{2'}$-type transition state with an elongated P−$O_{2'}$ bond (2.513 Å) and an almost fully formed P−$S_{5'}$ bond (2.537 Å) that is only 0.300 Å greater than that of the product structure. The $TS_{2'}$ transition state for S:$O_{5'}$ is a considerably later TS when compared to the $TS_{2'}$ transition states observed in the S:O_{P1} and S:O_{P1},O_{P2} reactions. Sulfur substitution at the leaving group 2′ position (S:$O_{2'}$) leads to a single early $TS_{5'}$-type transition state with an elongated P−$O_{5'}$ bond (2.757 Å) with considerable axial distortion of the trigonal bipyramid (θ_{ax} = 161.1°).

3.1.2. Gas-Phase Thermodynamics and Kinetics. Table 3 summarizes the key thermodynamic data for the dianionic reactions in the gas phase and in solution. In the gas phase, the reactions have very high activation energy barriers ($\Delta E^{\ddagger}$) that range from 77.3 (S:$O_{3'}$) to 99.4 (S:$O_{2'}$) kcal/mol, due mainly to the unscreened Coulombic repulsion between the two negatively charged ions. The reaction energy values (ΔE) are similarly positive, ranging from 12.0 to 73.7 kcal/mol, reflecting the preference for the repulsive ions to be infinitely separated. The gas-phase activation free energy barriers ($\Delta G^{\ddagger}$) and reaction free energy values (ΔG) are typically about 10−12 kcal/mol higher

TABLE 2: Structural Characterization of Stationary Points for Native and Thiosubstituted In-Line Monoanionic Mechanism of Ethylene Phosphate Methanolysis in the Gas Phase[b]

		monoanionic/monoprotic					
reaction	structure	$r(P-X_{5'})$	$r(P-X_{2'})$	θ_{ax}	$r(H-X_{5'/2'})$	$r(H-X_{P2})$	θ_{PT}
native	R	3.845	1.696	127.7	0.989	1.750	173.7
	$TS_{5'}$	2.261	1.717	159.4	1.460	1.052	134.5
	$I_{5'}$	1.789	1.780	160.4	1.929	0.969	100.8
	TS_{rot}	1.743	1.819	161.2	2.796	0.966	52.8
	$I_{2'}$	1.706	2.002	160.9	1.840	0.975	111.9
	$TS_{2'}$	1.689	2.148	160.4	1.748	0.985	120.3
	P	1.653	3.445	133.2	0.994	1.734	166.9
$S:O_{P1}$	R	3.998	1.690	133.0	0.985	1.773	174.2
	$TS_{5'}$	2.268	1.713	160.3	1.434	1.061	135.2
	$I_{5'}$	1.771	1.764	160.8	1.937	0.969	99.6
	TS_{rot}	1.727	1.791	160.9	2.781	0.967	52.7
	$I_{2'}$	1.702	1.923	160.8	1.885	0.972	107.4
	$TS_{2'}$	1.673	2.251	158.8	1.668	0.998	126.8
	P	1.649	3.467	131.4	0.990	1.765	166.3
$S:O_{P1},O_{P2}$	R	4.426	1.696	150.1	0.979	2.395	172.8
	$TS_{5'}$	2.064	1.741	159.9	1.374	1.505	129.3
	$I_{5'}$	1.741	1.790	158.5	2.263	1.347	92.9
	TS_{rot}	1.726	1.787	159.5	3.170	1.346	57.9
	$I_{2'}$	1.730	1.829	160.4	2.275	1.347	96.3
	$TS_{2'}$	1.682	2.300	159.8	1.572	1.421	130.9
	P	1.654	3.721	136.0	0.983	2.347	169.2
$S:O_{3'}$	R	3.843	1.681	120.4	0.986	1.776	172.8
	$TS_{5'}$	2.307	1.698	157.3	1.497	1.044	135.4
	$I_{5'}$	1.823	1.762	160.7	1.944	0.970	102.1
	TS_{rot}	1.771	1.803	162.3	2.860	0.967	52.0
	$I_{2'}$	1.733	1.930	162.8	1.921	0.972	107.4
	$TS_{2'}$	1.695	2.222	160.4	1.686	0.994	125.0
	P	1.661	3.522	142.1	0.992	1.748	171.2
$S:O_{5'}$	R	4.196	1.696	132.7	1.370	1.921	170.8
	$TS_{5'}$						
	$I_{5'}$						
	TS_{rot}	2.298	1.771	156.3	3.144	0.968	55.0
	$I_{2'}$	2.263	1.897	160.8	1.916	0.973	105.6
	$TS_{2'}$	2.197	2.231	159.7	1.666	1.001	126.1
	P	2.153	3.458	133.9	0.992	1.749	166.2
$S:O_{2'}$	R	3.843	2.221	135.5	0.986	1.776	172.8
	$TS_{5'}$	2.236	2.256	160.3	1.439	1.062	134.3
	$I_{5'}$	1.759	2.393	161.7	1.961	0.972	98.9
	TS_{rot}	1.675	3.189	163.6	2.147	0.971	92.8
	$I_{2'}$						
	$TS_{2'}$						
	P	1.634	3.737	126.4	1.799	1.116	173.2

[b] Distance quantities (r) are in Å, and angular quantities (θ) are in degrees. The angular quantity θ_{ax} is the axial $X_{5'}-P-X_{2'}$ angle, and the angular quantity θ_{PT} is the proton transfer $X_{5'/2'}-H-X_{P2}$ angle. Here $X_{5'/2'}$ designates the $X_{5'}$ atom for the R, $TS_{X5'}$, and $I_{X5'}$ structures, and designates the $X_{2'}$ atom for the $I_{X2'}$, $TS_{X2'}$, and P structures.

than the corresponding adiabatic energy values for all the reactions, which reflects the loss of translational and rotational freedom in the dianionic complexes relative to the reactant molecules at infinite separation.

Substitution at the Equatorial 3′ and Nonbridging Phosphoryl Positions. The native reaction has an activation free energy energy barrier of 98.3 kcal/mol and a reaction free energy of 56.6 kcal/mol in the gas phase. Single sulfur substitution at the nonbridging phosphoryl position ($S:O_{P1}$) leads to a decrease in the activation free energy barrier by 5.3 kcal/mol, and double sulfur substitution at the nonbridging positions ($S:O_{P1},O_{P2}$) leads to a decrease by 8.0 kcal/mol. The decrease in gas-phase activation free energy upon sulfur substitution at the nonbridging positions is mainly enthalpic in nature. Because the nonbridging O_{P1} and O_{P2} positions carry the majority of the negative charge, (which increases in anionic character upon moving to the transition state), the softer, more polarizable sulfur in the nonbridging position can facilitate redistribution of the charge and stabilization of the dianionic transition state. Hence, the $\Delta H^{\ddagger}$ values for the $S:O_{P1}$ and $S:O_{P1},O_{P2}$ reactions decrease relative to the value for the native reaction due to electronic stabilization of the dianionic transition state by the softer sulfur atoms at the nonbridging positions.

Substitution at the $O_{3'}$ position leads to a decrease in the forward activation free energy by 8.9 kcal/mol that derives mainly from the lower enthalpy of activation. The sulfur substitution at the 3′ position has a stabilizing electronic effect in the dianionic transition state as discussed above for the nonbridging substitutions. As has been pointed out by others, 3′ substitution can lead to geometric changes in the backbone that result from elongated bonds and sharpened angles, and hence the cyclic transition state can be stabilized by relief of the strain energy in the five-membered ring.[15,84,85] Although this effect may be important, relief of ring strain of the 3′ thiosubstituted cyclic phosphate in the phosphorane transition state does not completely account for the observed lowering of both the forward and reverse reaction barriers. If relief of ring strain were the only factor at play, then only the forward barrier

TABLE 3: Gas-Phase Thermodynamic Data and Solvation Free Energy Values for Stationary Points for Native and Thiosubstituted In-Line Dianionic Mechanism of Ethylene Phosphate Methanolysis[3]

		gas phase				$\Delta\Delta G_{sol}$			ΔG_{aq}		
reaction	structure	ΔE	ΔH	$-T\Delta S$	ΔG	PCM	CPCM	SM5	PCM	CPCM	SM5
native	$TS_{5'}$	87.2	87.1	11.2	**98.3**	−57.2	−58.3	−68.1	**41.1**	**40.0**	**30.2**
	I										
	$TS_{2'}$										
	P	44.1	46.5	10.1	56.6	−43.8	−42.7	−49.5	12.8	13.9	7.1
$S{:}O_{P1}$	$TS_{5'}$	82.4	82.5	10.5	**93.0**	−52.4	−54.0	−65.3	**40.6**	**39.0**	**27.7**
	I	74.5	76.5	11.8	88.3	−61.3	−62.9	−65.1	27.0	25.4	23.2
	$TS_{2'}$	74.9	76.0	12.2	88.2	−59.4	−61.4	−63.2	28.8	26.8	25.0
	P	42.1	44.5	9.5	54.0	−40.1	−39.2	−46.3	13.9	14.8	7.7
$S{:}O_{P1},O_{P2}$	$TS_{5'}$	79.6	79.8	10.5	**90.3**	−48.7	−50.5	−62.4	**41.6**	**39.8**	**27.9**
	I	66.2	68.8	12.2	81.0	−56.6	−58.0	−61.5	24.4	23.0	19.5
	$TS_{2'}$	68.8	70.1	12.4	82.5	−46.0	−45.6	−58.0	36.6	36.9	24.5
	P	39.7	42.2	10.0	52.2	−38.1	−36.8	−43.2	14.1	15.4	9.0
$S{:}O_{3'}$	$TS_{5'}$	77.3	77.8	11.6	**89.4**	−53.1	−52.7	−64.0	**36.3**	**36.7**	**25.4**
	I										
	$TS_{2'}$										
	P	42.4	44.7	8.8	53.5	−40.6	−39.2	−47.8	12.9	14.3	5.7
$S{:}O_{5'}$	$TS_{5'}$										
	I										
	$TS_{2'}$	99.4	98.0	10.1	**108.0**	−52.1	−54.2	−56.5	**55.9**	**53.8**	**51.5**
	P	73.7	73.8	9.2	82.9	−48.8	−49.1	−46.5	34.1	33.9	36.4
$S{:}O_{2'}$	$TS_{5'}$	78.5	78.8	9.2	**88.0**	−45.6	−46.3	−60.3	**42.4**	**41.7**	**27.7**
	I										
	$TS_{2'}$										
	P	12.0	16.0	9.4	25.4	−34.2	−32.5	−47.1	−8.8	−7.1	−21.7

[a] Relative thermodynamic quantities and solvation free energy values (kcal/mol) are with respect to the infinitely separated reactants. Solvation free energies were calculated with the PCM, CPCM, and SM5 solvation models (see text).

from the strained cyclic reactant would be significantly decreased, whereas it is observed from the calculations that also the reverse barrier from the acyclic product is also lowered considerably. This raises an interesting question: *how does the role of sulfur substitution at the 3′ position differ from that at the nonbridging positions?*

Insight into the different stabilizing role of sulfur at the nonbridging ($S{:}O_{P1}$ and $S{:}O_{P1},O_{P2}$) and bridging ($S{:}O_{3'}$) positions can be gleaned from differences in their reaction profiles. The activation energy barriers for the forward and reverse dianionic $S{:}O_{P1}$ and $S{:}O_{P1},O_{P2}$ reactions are decreased, and the rate-controlling $TS_{5'}$ transition states have less associative character relative to the native reaction. Substitution at the nonbridging positions produces a metastable dianionic phosphorane intermediate (I) in the gas phase that becomes increasingly stable with sulfur substitution. For single and double sulfur substitution, the energy barrier to collapse of the intermediate to the product state is 0.4 and 2.6 kcal/mol, respectively. In accord with the Hammond postulate,[86,87] stabilization of the intermediate lowers both the $TS_{5'}$ and $TS_{2'}$ barriers and shifts the location of these transition states away from the intermediate (i.e., toward that of reactants and products, for $TS_{5'}$ and $TS_{2'}$, respectively). For the rate-controlling $TS_{5'}$ transition state, this results in decreased associative character relative to the native reaction.

In contrast, sulfur substitution at the 3′ position does not produce an intermediate in the gas phase, but instead leads to reduced effective repulsion between the methoxide nucleophile and the thiophosphate, which increases the associative character of the methoxide nucleophile. The $TS_{5'}$ transition state in the $S{:}O_{3'}$ is stabilized relative to both the reactant and product state and leads to a considerable reduction of both the forward and reverse activation free energy barriers relative to the native reaction by −8.9 and −5.8 kcal/mol, respectively. Relief of ring strain is one of the factors leading to reduction of the forward reaction barrier. In particular, the $S_{3'}-P-O_{2'}$ and $P-S_{3'}-C$ angles of the reactant are contracted by 10.6° and 13.8°, respectively, relative to the $S_{3'}-P-O_{5'}$ and $P-S_{3'}-C$ angles of the acyclic product, whereas the corresponding contraction for the native reaction is 8.2° and 11.5°, respectively. Hence, destabilization of the reactant arising from ring strain that is alleviated upon formation of the transition state is one reason the forward barrier is reduced in the $S{:}O_{3'}$ reaction. Like the forward barrier, the reverse barrier from the acyclic product for $S{:}O_{3'}$ is lowered by 5.9 kcal/mol relative to the native reaction. That the forward barrier is lowered to a greater degree (3.1 kcal/mol lower versus the reverse barrier) suggests that ring strain is an important factor. The softer sulfur in the nonbridging position electronically stabilizes the dianionic $TS_{5'}$ transition state and reduces the effective repulsions in the exocyclic bond formation step. The longer $P-S_{3'}$ bond also allows a greater distance between the negatively charged phosphorothioate and the $O_{2'}$ leaving group for the $S{:}O_{3'}$ reaction ($P\cdots O_{2'}$ distance 5.66 Å) relative to the native reaction ($P\cdots O_{2'}$ distance 5.14 Å).

Substitution at the Nucleophilic 5′ and Leaving Group 2′ Positions. Sulfur substitution at the $O_{5'}$ position leads to a significantly increased forward activation free energy barrier in the gas phase by 9.7 kcal/mol relative to the native reaction due to the increased stability of the reactant thiolate anion. The effect on the reverse barrier is even more pronounced. The $S{:}O_{5'}$ reaction has a reverse activation free energy barrier (25.1 kcal/mol) that is 16.6 kcal/mol less than that of the native reaction in the gas phase. Unlike the other sulfur substitutions, the $S{:}O_{5'}$ substitution shifts the transition state to one having $TS_{2'}$ character. In other words, the enhanced leaving group character of the 5′ thiolate (which is particularly reticent toward nucleophilic attack to phosphate centers), raises the barrier for exocyclic bond formation, and in accord with the Hammond postulate, shifts the transition state character toward that of endocyclic cleavage leading to the product state.

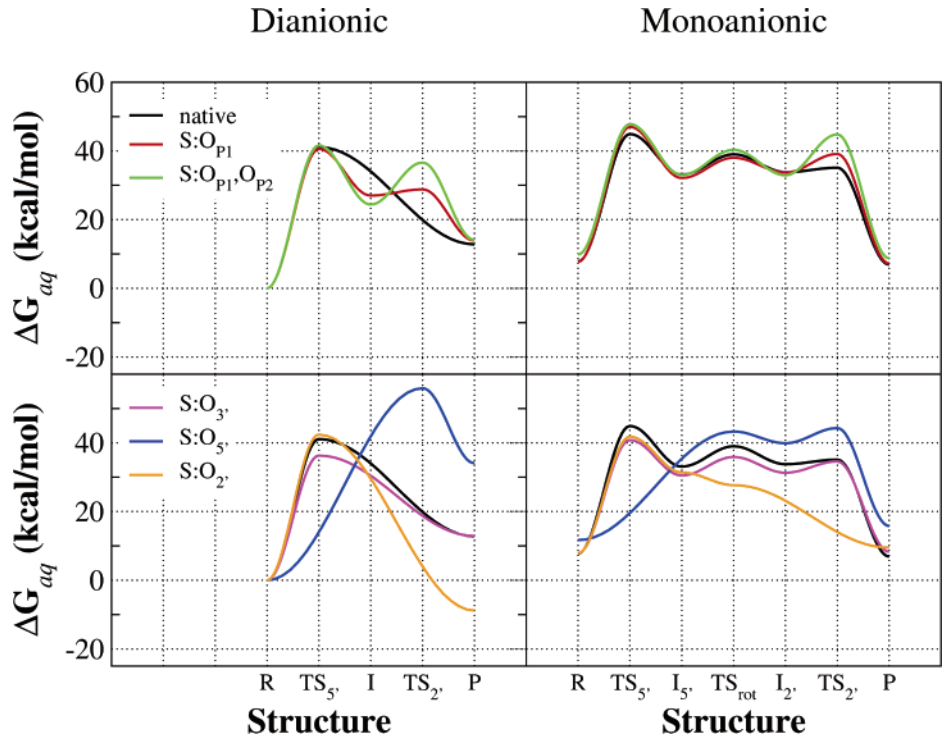

Figure 1. Free energy profiles for dianionic (left) and monoanionic (right) native and thiosubstituted ethylene phosphate methanolysis reactions with PCM solvation model.

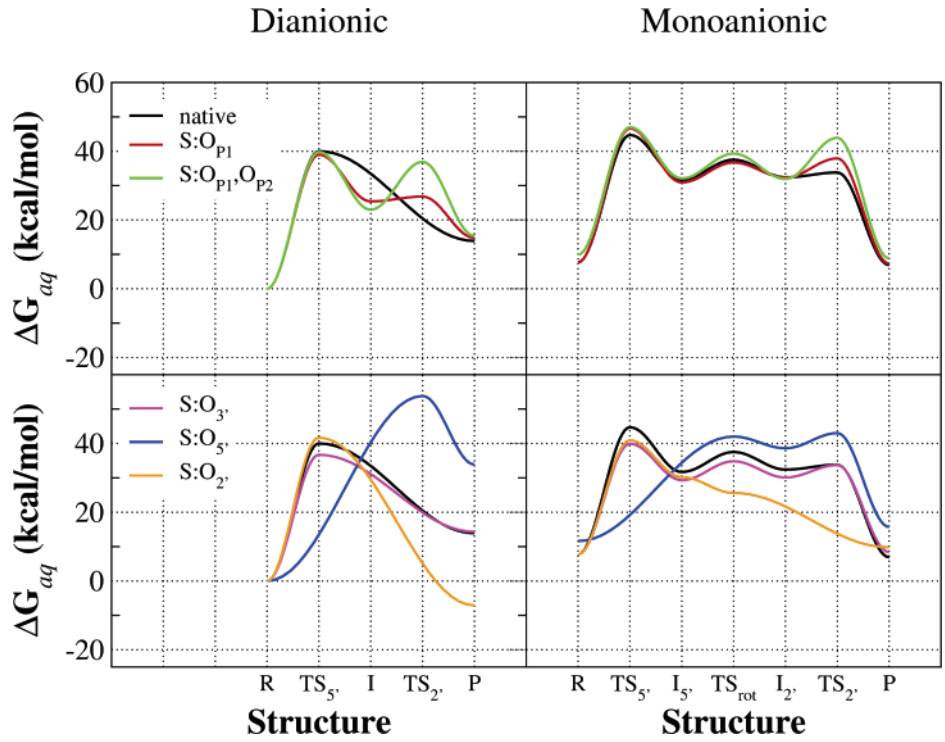

Figure 2. Free energy profiles for dianionic (left) and monoanionic (right) native and thiosubstituted ethylene phosphate methanolysis reactions with CPCM solvation model.

Sulfur substitution at the $O_{2'}$ position behaves conversely to that of $S:O_{5'}$ reaction. The forward free energy barrier in the gas phase is lowered by 10.3 kcal/mol relative to the native reaction due to increased stabilization of the 2′ substituted thiolate product. The transition state is shifted along the reaction coordinate toward that of the reactants, and hence becomes less associative. Conversely, the reverse free energy barrier in the gas phase (62.6 kcal/mol) is elevated by 20.9 kcal/mol relative to the native reaction. Hence, the dominant effect of 5′/2′ sulfur substitution in the gas phase involves the increased stability of the thiolate nucleophile/leaving group.

3.1.3. Solvation Free Energy Profiles. Figures 1, 2, and 3 illustrate the free energy profiles for in-line methanolysis of native and thiosubstituted ethylene phosphate. In Table 3, the relative solvation energies ($\Delta\Delta G_{sol}$) and aqueous free energy (ΔG_{aq}) values for stationary points of the dianionic reactions are listed. The solvation energies calculated with the PCM, CPCM, and SM5 methods exhibit mild variations, but overall

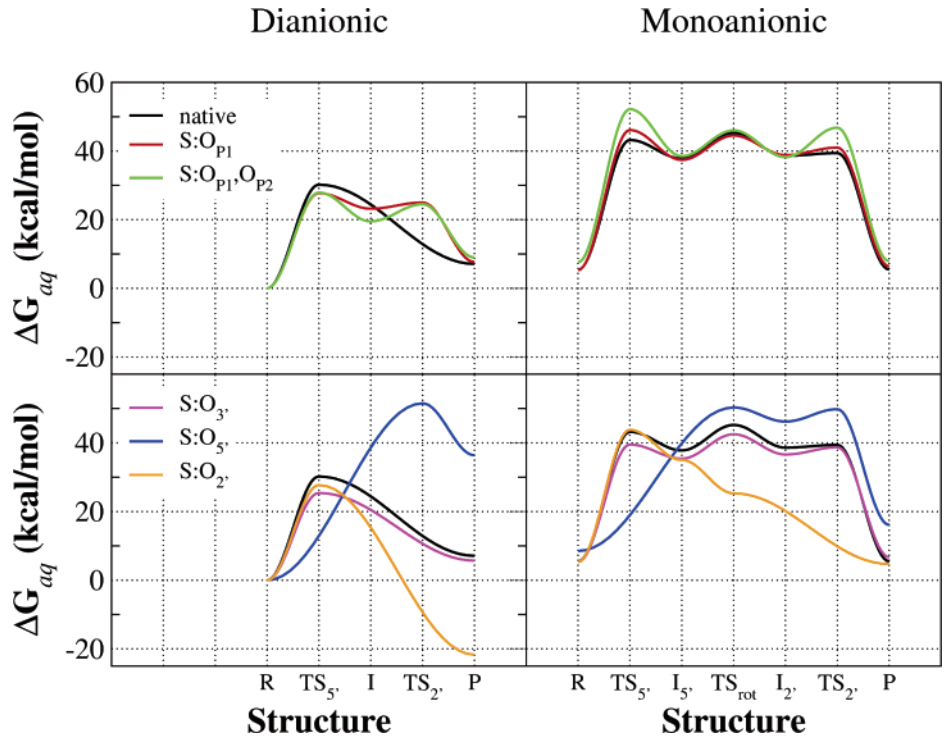

Figure 3. Free energy profiles for dianionic (left) and monoanionic (right) native and thiosubstituted ethylene phosphate methanolysis reactions with SM5 solvation model.

produce a consistent picture of the solvation effect and general trends. Consequently, reference to specific solvation energy values in this section will be restricted to the PCM results unless otherwise explicitly indicated.

For dianionic reactions, the solvation free energy for the separate monoanionic reactants are significantly less favorable than those of the dianionic transition states, intermediates, and product. The large favorable solvation of the dianionic transition states leads to a significant reduction of the activation barrier in solution. The rate-controlling $TS_{5'}$ transition state for the native reaction has the largest solvation free energy (−57.2 kcal/mol) compared with the rate-controlling transition state for the sulfur-substituted reactions. Because the nonbridging O_{P1} and O_{P2} atoms carry the majority of the dianionic charge and are more sensitive to substitution by the larger sulfur atoms than the $O_{3'}$ atom, the rate-controlling transition state for the S:O_{P1} and S:O_{P1},O_{P2} reactions have less favorable solvation free energy values (−52.4 and −48.7 kcal/mol, respectively) than that of the S:$O_{3'}$ reaction (−53.1 kcal/mol). The solvation free energy values for the rate-controlling transition states for the S:$O_{5'}$ and S:$O_{2'}$ reactions are −52.1 and −45.6 kcal/mol, respectively.

In solution, the calculated results suggest the rate-controlling transition state for the native reaction corresponds to the formation of the P−$O_{5'}$ bond and has a activation free energy energy barrier of 41.1 kcal/mol and a reaction free energy of 12.8 kcal/mol. The S:O_{P1} reaction and the S:O_{P1},O_{P2} reactions both exhibit two transition states corresponding to the formation of the P−$O_{5'}$ bond ($TS_{5'}$) and the cleavage of the P−$O_{2'}$ bond ($TS_{2'}$). The rate-controlling step is the formation of the exocyclic P−$O_{5'}$ bond with a free energy barrier of 40.6 kcal/mol for single substitution and 41.6 kcal/mol for double substitutions, which is higher than the endocyclic cleavage barrier by 11.8 and 5.0 kcal/mol, respectively. Single and double sulfur substitution at the nonbridging positions thus have only a small effect on the activation barrier and the reaction free energy compared with the native reaction. Substitution at the bridging $O_{3'}$ position leads to a decrease in the activation barrier by 4.8 kcal/mol. Thio substitution at the $O_{2'}$ position leads to a slight increase in the activation barrier and a decrease of 21.6 kcal/mol in the reaction free energy. This considerably raises the barrier of the reverse reaction. Thio substitution at the $O_{5'}$ position results in the largest activation barrier (55.9 kcal/mol) and reaction free energy (34.1 kcal/mol). This is largely due to the increased stability of the thiolate nucleophile in solution (methanethiol has a pK_a value 5 units lower than methanol[88]).

3.2. Monoanionic Reactions. Scheme 3 illustrates the general mechanism for monoanionic/monoprotic in-line methanolysis of ethylene phosphate, with phosphoryl oxygen positions labeled in accord with their RNA counterparts involved in RNA transesterification (Scheme 1).

3.2.1. Structure and Mechanism. The key structural parameters for stationary points along the monoanionic reaction mechanisms are listed in Table 2. Unlike the dianionic reactions, the monoanionic reactions all show stable reactant hydrogen bonded complexes, the weakest being for the S:$O_{5'}$ reaction where the hydrogen bond donor is methanethiol. The monoanionic/monoprotic $I_{5'}$ and $I_{2'}$ phosphorane intermediates have considerably distorted $O_{5'}$−P−$O_{2'}$ angles (θ_{ax} values range from 158.5 to 162.8°).

The native, S:$O_{3'}$, S:O_{P1}, and S:O_{P1},O_{P2} reactions have qualitatively similar stationary point geometries along the reaction path and proceed via an $A_N + D_N$-type mechanism.[89] The S:O_{P1},O_{P2} reaction has the largest degree of associative character in the rate-controlling $TS_{5'}$ transition state (P−$O_{5'}$ bond length 2.064 Å), and the most elongated P−$O_{2'}$ bond (2.300 Å) in $TS_{2'}$. The S:$O_{5'}$ reaction does not exhibit a $TS_{5'}$-type transition state corresponding to exocyclic bond formation, and similarly, the S:$O_{2'}$ reaction does not produce a $TS_{2'}$-type transition state corresponding to endocyclic bond cleavage.

With the exception of the S:O_{P1},O_{P2} reaction, the proton transfer in the $TS_{5'}$ transition states is nearly complete, as the distance between the proton and the $O_{5'}$ of the nucleophile (1.434−1.497 Å) is significantly longer than the distance

TABLE 4: Gas-Phase Thermodynamic Data and Solvation Free Energy Values for Stationary Points for Native and Thiosubstituted In-Line Monoanionic Mechanism of Ethylene Phosphate Methanolysis[a]

		gas phase				$\Delta\Delta G_{sol}$			ΔG_{aq}		
reaction	structure	ΔE	ΔH	$-T\Delta S$	ΔG	PCM	CPCM	SM5	PCM	CPCM	SM5
native	R	−14.7	−13.2	8.4	−4.9	12.7	12.6	10.3	7.8	7.7	5.4
	$TS_{5'}$	22.4	21.1	12.2	33.3	11.6	11.3	9.9	**44.9**	**44.7**	43.2
	$I_{5'}$	13.7	14.8	13.1	27.9	5.3	3.8	9.9	33.1	31.7	37.8
	TS_{rot}	22.6	22.5	13.1	**35.6**	3.4	2.0	9.6	39.0	37.5	45.2
	$I_{2'}$	13.8	14.7	12.6	27.3	6.6	5.1	11.3	33.8	32.4	38.6
	$TS_{2'}$	13.8	13.9	13.4	27.3	7.9	6.5	12.1	35.1	33.8	39.4
	P	−18.4	−16.9	11.4	−5.5	12.4	12.4	11.0	6.9	6.9	5.5
$S:O_{P1}$	R	−13.1	−11.7	7.8	−3.9	11.6	11.5	9.2	7.7	7.6	5.3
	$TS_{5'}$	25.9	24.3	12.3	**36.6**	10.4	10.0	9.5	**47.0**	**46.6**	**46.1**
	$I_{5'}$	14.2	15.4	12.8	28.1	4.0	2.7	9.3	32.1	30.9	37.4
	TS_{rot}	22.0	22.0	12.8	34.9	3.1	1.9	9.6	38.0	36.7	44.5
	$I_{2'}$	15.3	16.3	12.4	28.7	5.0	3.6	10.1	33.7	32.3	38.8
	$TS_{2'}$	16.2	16.1	13.1	29.2	9.9	8.7	11.8	39.1	37.9	41.0
	P	−17.2	−15.7	11.3	−4.3	11.6	11.6	10.7	7.2	7.3	6.4
$S:O_{P1},O_{P2}$	R	−9.4	−8.1	7.8	−0.3	10.1	10.2	7.9	9.8	9.9	7.6
	$TS_{5'}$	33.9	30.9	12.4	**43.2**	4.6	3.8	9.0	**47.8**	**47.0**	**52.2**
	$I_{5'}$	17.3	16.5	12.5	29.1	3.9	3.1	9.4	33.0	32.1	38.5
	TS_{rot}	25.1	23.5	12.7	36.3	4.0	3.1	9.8	40.3	39.3	46.0
	$I_{2'}$	18.0	17.2	12.0	29.1	3.8	2.8	9.1	32.9	31.9	38.2
	$TS_{2'}$	26.1	23.4	13.1	36.5	8.3	7.4	10.3	44.8	43.9	46.8
	P	−13.8	−12.3	10.9	−1.5	10.1	10.2	9.4	8.7	8.8	7.9
$S:O_{3'}$	R	−13.4	−12.0	8.0	−4.0	11.8	11.7	9.3	7.9	7.7	5.3
	$TS_{5'}$	19.5	18.2	12.1	30.4	10.4	9.6	9.1	**40.8**	**39.9**	39.5
	$I_{5'}$	13.1	14.0	12.5	26.5	4.0	2.8	8.9	30.5	29.3	35.4
	TS_{rot}	21.8	21.6	12.6	**34.2**	1.7	0.6	8.3	35.9	34.8	**42.5**
	$I_{2'}$	15.4	16.0	11.8	27.8	3.5	2.3	8.8	31.3	30.1	36.6
	$TS_{2'}$	16.3	15.9	12.7	28.6	6.0	5.1	10.1	34.6	33.7	38.7
	P	−14.3	−13.0	10.6	−2.4	10.7	10.8	9.1	8.3	8.4	6.7
$S:O_{5'}$	R	−10.3	−9.0	8.8	−0.3	12.0	11.8	8.8	11.7	11.6	8.5
	$TS_{5'}$										
	$I_{5'}$										
	TS_{rot}	26.6	28.0	11.6	**39.6**	3.7	2.4	10.7	43.3	42.0	**50.3**
	$I_{2'}$	20.3	22.6	12.0	34.6	5.3	4.0	11.6	39.9	38.6	46.2
	$TS_{2'}$	21.9	23.1	12.9	36.0	8.3	7.0	13.8	**44.3**	**43.0**	49.8
	P	−10.7	−7.7	10.9	3.2	12.6	12.5	12.9	15.8	15.7	16.1
$S:O_{2'}$	R	−13.4	−12.0	8.0	−4.0	11.8	11.7	9.3	7.9	7.7	5.3
	$TS_{5'}$	25.4	23.9	11.0	**34.9**	6.9	6.0	8.9	**41.8**	**40.9**	**43.8**
	$I_{5'}$	13.9	14.8	12.2	27.0	4.5	3.2	8.0	31.4	30.2	35.0
	TS_{rot}	15.2	15.5	11.6	27.0	0.6	−1.5	−1.7	27.7	25.6	25.3
	$I_{2'}$										
	$TS_{2'}$										
	P	−13.3	−14.3	10.9	−3.4	12.86	13.15	8.06	9.5	9.8	4.7

[a] Relative thermodynamic quantities and solvation free energy values (kcal/mol) are with respect to the infinitely separated reactants. Solvation free energies were calculated with the PCM, CPCM, and SM5 solvation models (see text).

between the proton and the nonbridging phosphoryl oxygen (1.044−1.062 Å). The situation is even more pronounced for the $TS_{2'}$ transition state in that the distance between the proton and the nonbridging phosphoryl oxygen (0.985−1.001 Å) is essentially a fully formed single bond, and the distance from the proton to the $O_{2'}$ leaving group is in the range of a short hydrogen bond (1.666−1.748 Å). Hence, the proton transfer has more concerted character in the $TS_{5'}$ transition states (particularly for the $S:O_{P1}$ reaction), whereas it is essentially stepwise in the $TS_{2'}$ transition states. The exception is for the $S:O_{P1},O_{P2}$ reaction, where the proton must be transferred to a nonbridging phosphoryl sulfur. In this case, the proton transfer in $TS_{5'}$ is more highly bonded to the $O_{5'}$ nucleophile (1.374 Å) and less fully bonded to the nonbridging position (1.505 Å) than in the native reaction. Proton transfer in $TS_{2'}$ for the $S:O_{P1},O_{P2}$ reaction exhibits a less fully formed $H-O_{2'}$ bond (1.572 Å) to the leaving group than in $TS_{5'}$, but this bond is still more fully formed than the corresponding $TS_{2'}$ values for the other reactions. Overall, the proton transfer for $S:O_{P1},O_{P2}$ is the most highly concerted with exocyclic bond formation ($TS_{5'}$) and endocyclic cleavage ($TS_{2'}$).

3.2.2. Gas-Phase Thermodynamics and Kinetics. Table 4 summarizes the key thermodynamic data for the monoanionic reactions in the gas phase and in solution. The gas-phase activation energy barriers ($\Delta E^{\ddagger}$) range from 21.8 ($S:O_{3'}$) to 33.9 ($S:O_{P1},O_{P2}$) kcal/mol and are considerably lower than those of the dianionic reactions due to alleviation of the electrostatic repulsion between negatively charged ions in the gas phase. The reaction energy values (ΔE) are negative in all cases, ranging from −10.7 ($S:O_{5'}$) to −18.4 (native) kcal/mol, in contrast to the large positive values observed for the dianionic reactions. The gas-phase activation free energy barriers ($\Delta G^{\ddagger}$) and reaction free energy values (ΔG) are typically about 9−10 kcal/mol higher than the corresponding adiabatic energy values for all the reactions.

In gas phase, the potential energy surface is significantly lower for the monoanionic reactions than for the dianionic reactions. This is due to the alleviation of unfavorable repulsion

between the negatively charge ions in the gas phase. Unlike the dianionic reactions, the monoanionic reactions exhibit significantly stable reactant hydrogen bonded complexes with binding free energy values that range from −3.9 to −4.9 kcal/mol when both the hydrogen bond donor and acceptor are oxygen. For the $S:O_{5'}$ and $S:O_{P1},O_{P2}$ reactions, the hydrogen bond donor and acceptor, respectively, involve sulfur, and the reactant binding free energy is reduced to only −0.3 kcal/mol.

For the native reaction, the gas-phase activation free energy barrier (TS_{rot}) is 35.6 kcal/mol, and reaction free energy is −5.5 kcal/mol. Single ($S:O_{P1}$) and double ($S:O_{P1},O_{P2}$) sulfur substitution leads to an increase in the $\Delta G^{\ddagger}$ value by 1.0 and 7.6 kcal/mol, respectively. Sulfur substitution destabilizes hydrogen bonding, and hence the free energy difference in going from the reactant hydrogen bonded complexes to the rate-controlling transition state is more uniform for the native, $S:O_{P1}$, and $S:O_{P1},O_{P2}$ reactions. The $S:O_{P1},O_{P2}$ reaction has particularly high-energy phosphorane intermediate and transition states due to the less favorable protonation of a nonbridging sulfur as opposed to oxygen.

Substitution at the $O_{3'}$ position leads to a decrease in the activation free energy relative to the native reaction by 1.4 kcal/mol. For the monoanionic reaction, the electronic effect of sulfur at the 3′ position is small, and the dominant stabilization effect involves alleviation of ring strain in going from the monoanionic cyclic phosphorothioate to the cyclic thiophosphorane.[15]

Sulfur substitution at the $O_{5'}$ position leads to only a moderately increased activation free energy barrier relative to the native reaction by 4.0 kcal/mol, and an increased reaction free energy by 8.7 kcal/mol. This primarily derives from the lower proton affinity of methanethiol relative to methanol (the calculated proton affinity of methanol is 21.2 kcal/mol greater than that for methanethiol) and complete elimination of the $TS_{5'}$ transition state. Sulfur substitution at the $O_{2'}$ position, on the other hand, lowers the activation free energy barrier relative to the native reaction by 0.7 kcal/mol while raising the reaction free energy by 2.1 kcal/mol. The enhanced leaving group ability of sulfur eliminates the $TS_{2'}$ transition state.

3.2.3. Solvation Free Energy Profiles. Figures 1, 2, and 3 illustrate the free energy profiles for in-line methanolysis of native and thiosubstituted ethylene phosphate. Relative solvation energies ($\Delta\Delta G_{sol}$) and aqueous free energy (ΔG_{aq}) values for stationary points of the dianionic reactions are listed in Table 4. As for the dianionic reactions, those calculated with the PCM, CPCM, and SM5 methods exhibit mild variations, but overall produce a consistent picture of the solvation effect and general trends. Consequently, reference to specific solvation energy values in this section will be restricted to the PCM results unless otherwise explicitly indicated.

The solvation free energy values for the monoanionic reactions, and preferential stabilization of the transition states and intermediates, are not nearly as pronounced as those for the dianionic reactions. For the monoanionic reactions, the solvation free energy for the separated reactants are slightly more favorable than that of the transition states, intermediates, and the product, and are of opposite sign to and more than half an order of magnitude smaller than corresponding values for the dianionic reactions. The effect of solvation for the monoanionic reactions is to raise the aqueous activation free energy barriers by about 5−10 kcal/mol. In the native reaction, the barrier is shifted from that of a TS_{rot} in the gas phase to that of a $TS_{5'}$ in the aqueous phase, and raises the $TS_{5'}$ barrier relative to the gas phase by 11.6 kcal/mol. The solvation effect on the rate-controlling transition state is less pronounced for the $S:O_{P1}$ and $S:O_{P1},O_{P2}$ reactions, as well as the $S:O_{3'}$ reaction, due to the larger sulfur atoms.

The rate-controlling transition state of the $S:O_{5'}$ reaction in solution shifts from proton rotation (TS_{rot}) to the endocyclic bond cleavage ($TS_{2'}$) for the PCM and CPCM solvation models, but not for the SM5 solvation model. The $TS_{2'}$ aqueous activation free energy barrier is raised by 8.3 kcal/mol relative to the gas-phase value. Solvation has the smallest effect on the $S:O_{2'}$ reaction, causing only a modest increase the aqueous activation free energy barrier by 6.9 kcal/mol relative to the gas-phase value.

In solution, the monoanionic native reaction has a rate-controlling $TS_{5'}$ transition state with an activation free energy energy barrier of 44.9 kcal/mol and reaction free energy of 6.9 kcal/mol. Single and double thiosubstitution at the nonbridging positions leads to an increase on the aqueous activation free energy barrier by 2.1 and 2.9 kcal/mol, respectively. Thiosubstitution at the $O_{3'}$ position results in a decrease in the aqueous activation free energy barrier by 4.1 kcal/mol relative to the native reaction. Thio substitution at the $O_{2'}$ position leads to a decrease in the activation free energy barrier by 3.1 kcal/mol and an increase in the reaction free energy by 2.6 kcal/mol. Substitution at the $O_{5'}$ position lowers the activation free energy barrier by 0.6 kcal/mol and raises the reaction free energy barrier by 8.9 kcal/mol.

4. Discussion

4.1. Reliability of Solvation Models. Solvent effects are of paramount importance for the series of reactions in the present work. This is especially the case for the dianionic reactions, where solvent stabilization reduces the activation free energy barriers by typically 40−60 kcal/mol. Consequently, it is important to, where possible, provide some assessment as to the typical accuracy of the solvation models for the systems under study. Unfortunately, there are few experimental solvation free values available for relevant phosphate and phosphorothioate molecules to provide direct comparison. Table 5 summarizes the experimental and calculated solvation free energy values for the most relevant set of oxygen and sulfur-containing molecules and related anions that pertain to the reactions of the present work. Experimental values were taken from the database of solvation free energy values used to construct the SM5.42R universal solvation model[77] (see also refs 90−93).

For neutral molecules, SM5 performs the best with a mean unsigned error (MUE) of 0.42 kcal/mol, whereas the PCM and CPCM models have larger values around 1.3 kcal/mol. A considerable component of the MUE for the PCM and CPCM methods derives from a systematic underprediction of the solvation free energy values for the set of neutral molecules in Table 6. The main source of error for the PCM and CPCM methods arises from the neutral phosphate triesters, where the solvation free energy values are considerably underpredicted by 4−5 kcal/mol. For the monoanions, the error for all the methods is considerably larger. The MUE error values are 8.0, 4.3, and 7.2 kcal/mol for PCM, CPCM, and SM5 methods, respectively. The CPCM method overall has the best agreement for the monoanionic solvation free energy values and also the smallest root-mean-square error (RMSE) of 5.2 kcal/mol compared with 9.2 and 8.8 kcal/mol for PCM and SM5, respectively. The PCM method has the largest error for the monoanions; however, this error is quite systematic, as observed by the dominant mean signed error (MSE) of 7.8 kcal/mol (standard deviation 4.9 kcal/mol). The SM5 model, on the other hand, exhibits a much smaller MSE (0.3 kcal/mol) but the largest

TABLE 5: Comparison of Calculated Solvation Free Energies with the PCM, CPCM, and SM5 Solvation Models with Experimental Values[a]

	exp.	PCM	CPCM	SM5
		Neutrals		
H_2O	−6.31	−5.97	−6.08	−5.96
CH_3OH	−5.11	−5.01	−5.14	−5.39
C_2H_5OH	−5.01	−5.39	−5.56	−5.43
C_3H_7OH	−4.83	−4.55	−4.75	−4.80
$(CH_3)_2CHOH$	−4.76	−5.18	−5.40	−4.62
CH_3SH	−1.24	−1.06	−1.10	−0.99
C_2H_5SH	−1.30	−1.73	−1.75	−1.05
C_6H_5OH	−6.62	−6.49	−6.81	−6.64
C_6H_5SH	−2.55	−1.89	−2.01	−2.77
$OP(OCH_3)_3$	−8.70	−3.59	−3.87	−7.48
$OP(OC_2H_5)_3$	−7.80	−4.18	−4.54	−6.69
$OP(OC_3H_7)_3$	−6.10	−1.70	−2.06	−5.34
MAXE		5.11	4.83	1.22
RMSE		2.23	2.07	0.57
MUE		1.34	1.25	0.42
MSE		1.13	0.94	0.26
		Anions		
HO^-	−106.60	−100.17	−109.90	−108.29
HS^-	−74.00	−68.51	−73.87	−84.40
CH_3O^-	−96.90	−80.59	−87.23	−83.90
CH_3S^-	−75.70	−67.78	−72.82	−76.71
$C_6H_5O^-$	−73.80	−62.54	−66.48	−62.06
$C_6H_5S^-$	−65.30	−57.39	−61.30	−63.63
$H_2PO_4^-$	−63.50	−64.45	−66.61	−74.56
MAXE		16.31	9.67	13.00
RMSE		9.18	5.24	8.82
MUE		8.04	4.34	7.22
MSE		7.77	2.51	0.32

[a] Shown are experimental and calculated solvation free energy values in kcal/mol. Experimental values were taken from the database of solvation free energy values used to construct the SM5.42R universal solvation model[77] (see also refs 90−93).

variation (standard deviation 8.8 kcal/mol). This larger variation is particularly large for $H_2PO_4^-$, where SM5 predicts a solvation free energy 11.1 kcal/mol too large in magnitude (more negative in value), whereas it also predicts for CH_3O^- a solvation free energy 13 kcal/mol too small in magnitude (less negative in value). It should be noted, however, that the reference value used for the solvation free energy of $H_2PO_4^-$ [77] is not strictly an experimental number, and preliminary data suggest the true value may be considerably more negative. Overall, the SM5 model performs best for the thiolates, but exhibits important deviations for the corresponding alkoxides.

For the purposes of this work, it is important to have sufficiently robust solvation methods that provide reliable free energy profiles in solution that are internally consistent when comparing native and thiosubstituted reactions. Hence, the errors in the solvation models must be sufficiently systematic that cancellation of errors leads to increased accuracy in the relative free energy values. Although none of the implicit solvation methods provide extremely high-accuracy results, both the PCM and CPCM methods, for the systems studied in the present work, provide a similar overall level of robustness that allows at least a qualitative characterization of the reaction profiles. For instance, kinetic experiments of RNA degradation[94] by specific base catalysis of transesterification suggests an activation energy of 29.0 kcal/mol. This activation energy (although not a free energy) is quite close to the free energy of activation values in solution for the dianionic reaction (Table 6) predicted by PCM (28.3 kcal/mol), similar to the value predicted by CPCM (26.1 kcal/mol) and moderately comparable to the SM5 value (23.1 kcal/mol). On the other hand, previous QM/MM calculations of dianionic transesterification thio effects[95,96] using the MNDO/d Hamiltonian predicted a fairly low native free energy barrier of 18.0 kcal/mol. This suggests that the use of standard van der Waals from the CHARMM force field[97] in hybrid QM/MM calculations may lead to overstabilization of dianionic phosphorane structures. However, it is also possible that the barriers predicted by the PCM and CPCM models are too high due to understabilization of the dianionic transition states (see below). These results underscore the need for more complete, comprehensive study of prototype phosphoryl transfer reactions with new solvation and QM/MM models and detailed comparison with available experiment.

Comparison of native and thiosubstituted reactions additionally requires accurate relative solvation free energy values between alcohols, thiols, phosphates, and phosphorothioate analogues. In some cases in the present work, this is cause for concern. For instance, the relative experimental solvation free energy between methoxide and methanolthioate is 21.2 kcal/mol, whereas the PCM, CPCM, and SM5 models predict relative solvation free energy values of 12.8, 14.4, and 7.2 kcal/mol, respectively. Even more pronounced are the discrepancies between methoxide and dihydrogen phosphate, where the relative experimental solvation free energy value (33.4 kcal/mol) is considerably greater than the values predicted from the PCM, CPCM, and SM5 models (16.1, 20.6, and 9.3 kcal/mol, respectively). It is clear that improvement of the treatment of solvation as a function of reaction coordinate is necessary for the quantitative characterization of these reactions in solution. Alternate strategies include the use of carefully parametrized semiempirical quantum Hamiltonian models and MM van der Waals radii parametrized to reproduce high-level DFT results in the gas phase as well as experimental properties in solution such as solvation free energy values, proton affinities and gas-phase basicities, pK_a shifts and multiple pK_a values, and where possible, reaction rate constants. These areas are the focus of future efforts, for which the present work helps to establish benchmark DFT and solvation results. The benchmark DFT results can be further utilized to parametrize new-generation semiempirical models for QM/MM simulation.

4.2. Comparison of Thio Effects for Rate-Controlling Steps of Methanolysis and Transesterification.

4.2.1. Dianionic Reactions. The effect of each thiosubstitution on the rate-controlling free energy barrier for the dianionic in-line (forward) methanolysis reaction and the in-line (reverse) transesterification reaction is summarized in Table 6 (differences with respect to the native reaction are indicated in parentheses).

Dianionic Reactions in Gas Phase. In the gas phase, the native and thiosubstituted reactions all exhibit a higher (forward) barrier for the methanolysis than that for the (reverse) transesterification reaction. In the case of the native reaction, the forward methanolysis reaction has a gas-phase free energy barrier of 98.3 kcal/mol, whereas the reverse transesterification reaction free energy barrier is 41.7 kcal/mol. The larger forward barrier for the gas-phase dianionic reactions is preserved in the thiosubstituted reactions and arises from the large unscreened Coulomb repulsions between the anionic nucleophile and cyclic phosphate.

Thio substitution has a diverse influence on the gas-phase reaction barriers depending on the position of chemical modification. The largest changes in free energy barriers are found for the $S{:}O_{5'}$ and $S{:}O_{2'}$ reactions. Thio substitution at the leaving group position leads to lower cleavage barriers, whereas thio substitution at the nucleophilic position raises the barrier to nucleophilic attack (relative to the corresponding alkoxide). The

TABLE 6: Forward and Reverse Rate-Controlling Free Energy Barriers for Native and Thiosubstituted In-Line Dianionic Methanolysis Reactions in the Gas Phase and in Solution[a]

	$\Delta G^{\ddagger}$		$\Delta G^{\ddagger}_{aq}$					
			PCM		CPCM		SM5	
reaction	fwd	rev	fwd	rev	fwd	rev	fwd	rev
native	98.3 (0.0)	41.7 (0.0)	41.1 (0.0)	28.3 (0.0)	40.0 (0.0)	26.1 (0.0)	30.2 (0.0)	23.1 (0.0)
$S:O_{P1}$	93.0 (−5.3)	39.0 (−2.7)	40.6 (−0.5)	26.7 (−1.6)	39.0 (−1.0)	24.2 (−1.9)	27.7 (−2.5)	20.0 (−3.1)
$S:O_{P1},O_{P2}$	90.3 (−8.0)	38.1 (−3.6)	41.6 (0.5)	27.5 (−0.8)	39.8 (−0.2)	24.4 (−1.7)	27.9 (−2.3)	18.9 (−4.2)
$S:O_{3'}$	89.4 (−8.9)	35.9 (−5.8)	36.3 (−4.8)	23.4 (−4.9)	36.7 (−3.3)	22.4 (−3.7)	25.4 (−4.8)	19.7 (−3.4)
$S:O_{5'}$	108.0 (9.7)	25.1 (−16.6)	55.9 (14.8)	21.8 (−6.5)	53.8 (13.8)	19.9 (−6.2)	51.5 (21.3)	15.1 (−8.0)
$S:O_{2'}$	88.0 (−10.3)	62.6 (20.9)	42.4 (1.3)	51.2 (22.9)	41.7 (1.7)	48.8 (22.7)	27.7 (−2.5)	49.4 (26.3)

[a] Relative free energy values (kcal/mol) in the gas phase ($\Delta G^{\ddagger}$) and in solution ($\Delta G^{\ddagger}_{aq}$) for the rate-controlling transition state of the forward (fwd) dianionic reaction (i.e., relative to the reactants at infinite separation), and of the reverse (rev) dianionic reaction (i.e., relative to the product state). Shown in parentheses are the relative free energy differences ($\Delta\Delta G^{\ddagger}$ and $\Delta\Delta G^{\ddagger}_{aq}$) with respect to the native reaction.

largest barrier relaxation with respect to the native reaction that occurs upon thio substitution (−16.6 kcal/mol) occurs for the $S:O_{5'}$ transesterification reaction, and the largest barrier increase (20.9 kcal/mol) occurs for the $S:O_{2'}$ transesterification reaction.

Thio substitutions at the nonbridging phosphoryl oxygen positions also leads to significant gas-phase barrier relaxation for both the methanolysis and transesterification reactions. In the case of the forward methanolysis reaction, barrier relaxations of −5.3 and −8.0 kcal/mol are observed for single ($S:O_{P1}$) and double ($S:O_{P1}O_{P2}$) thio substitutions, respectively, at the nonbridging positions. In the case of the reverse transesterification reaction, the barrier relaxations are less pronounced with values of −2.7 and −3.6 kcal/mol for single and double thio substitutions, respectively. The origin of the barrier relaxation derives from electronic stabilization of the dianionic transition states by the softer sulfur ligands and manifests itself by the appearance of a stable intermediate (I) that serves to lower the flanking $TS_{2'}$ and $TS_{5'}$ free energy values and shift their reaction coordinate values away from the intermediate.

Thio substitution at the 3′ position has a barrier relaxation effect even greater that that of the nonbridging thio substitutions in the gas phase. For the forward methanolysis and reverse transesterification reactions, the barrier relaxation for the $S:O_{3'}$ reaction with respect to the native reaction is −8.9 and −5.8 kcal/mol, respectively. As discussed in Section 3.1.2, the origin of the barrier relaxation is a combination of electronic and ring strain effects.

Dianionic Reactions in Solution. Solvent has a tremendous stabilization effect for all the dianionic reactions, as discussed in Section 3.1.3. Sulfur substitution has both electronic and solvation effects. The former have been characterized in the discussion of the gas-phase reaction, and here the focus is on the solvation contribution. The larger sulfur atoms are less well solvated, and because solvation has a tendency to preferentially stabilize the dianionic transition states and lower the reaction barriers, thio substitution tends to produce a less pronounced solvent-induced lowering of the reaction barriers. Hence, the electronic and solvation effects that occur upon sulfur substitution have the tendency to cancel one another, and the effect is to either raise or lower the aqueous free energy barriers of the forward methanolysis and reverse transesterification reactions. In general, the effect of solvation is more pronounced for methanolysis than transesterification because the separated reactant anions in the former have significantly different solvation than the dianionic transition state. Hence, the thio effect for the transesterification reactions are dominated by the electronic component, and overall, a relaxation of the rate-controlling barrier is observed in solution for $S:O_{P1}$, $S:O_{P1}O_{P2}$, $S:O_{3'}$, and $S:O_{5'}$ reactions. Alternately, for the methanolysis reactions, some of the gas-phase trends are reversed in solution due to the larger role played by solvation. In particular, for the $S:O_{P1}O_{P2}$ and $S:O_{2'}$ methanolysis reactions, the rate-controlling barriers are both lowered by −8.0 and −10.3 kcal/mol, respectively, whereas in solution with the PCM model, they are both raised by 0.5 and 1.3 kcal/mol, respectively. The change in sign does not occur for the $S:O_{P1}O_{P2}$ with the CPCM model and does not occur for either reaction with the SM5 model, although the trend is maintained that solvation greatly counterbalances the large barrier lowering with respect to the native reaction observed in the gas phase. For aqueous dianionic transesterification, the $S:O_{3'}$ and $S:O_{5'}$ reactions exhibit the largest degree of barrier relaxation (−4.9 and −6.5 kcal/mol, respectively with the PCM solvation model). The only instance where the barrier is raised for aqueous dianionic transesterification is for the $S:O_{2'}$ reaction, which has an aqueous barrier enhancement of 22.9 kcal/mol that is 2.0 kcal/mol greater than that observed in the gas phase.

4.2.2. Monoanionic Reactions. The effect of each thiosubstitution on the rate-controlling free energy barrier for the monoanionic in-line (forward) methanolysis reaction and the in-line (reverse) transesterification reaction is summarized in Table 7 (differences with respect to the native reaction are indicated in parentheses).

Monoanionic Reactions in Gas Phase. In the gas phase, the native and thiosubstituted reactions have comparable rate-controlling barriers for methanolysis and transesterification, with the former generally slightly lower by around 2−5 kcal/mol (with the exception of the $S:O_{5'}$ reaction, see below). The native reaction has a forward gas-phase methanolysis barrier of 35.6 kcal/mol and a reverse gas-phase transesterification barrier of 41.1 kcal/mol. The difference between the forward and reverse barriers is due largely to a reactant state that has the nucleophile and substrate at infinite separation, whereas the product state is a stable hydrogen-bonded complex. If the forward methanolysis barrier were taken from the stable hydrogen-bonded complex (R) in the tables, the forward and reverse barriers would become more comparable in the gas phase.

Single thio substitution at the nonbridging phosphoryl oxygen position in the monoanionic reactions has only a minor effect on the reaction barrier for the methanolysis and transesterification. Double sulfur substitution, on the other hand, increases the methanolysis and transesterification barriers by 7.6 and 3.6 kcal/mol, respectively. This is partially due to the fact that, upon double sulfur substitution, the mechanism considered must proceed through a protonated nonbridging sulfur transition state, which is less favorable than one where a nonbridging oxygen is protonated. Among the monoanionic reactions involving sulfur substitutions at the equatorial positions, thio substitution at the

TABLE 7: Forward and Reverse Rate-Controlling Free Energy Barriers for Native and Thiosubstituted In-Line Monoanionic Methanolysis Reactions in the Gas Phase and in Solution[a]

	$\Delta G^{\ddagger}$		$\Delta G^{\ddagger}_{aq}$					
			PCM		CPCM		SM5	
reaction	fwd	rev	fwd	rev	fwd	rev	fwd	rev
native	35.6 (0.0)	41.1 (0.0)	44.9 (0.0)	38.0 (0.0)	44.7 (0.0)	37.8 (0.0)	45.2 (0.0)	39.7 (0.0)
S:O_{P1}	36.6 (1.0)	40.9 (−0.2)	47.0 (2.1)	39.8 (1.8)	46.6 (1.9)	39.3 (1.5)	46.1 (0.9)	39.7 (0.0)
S:O_{P1},O_{P2}	43.2 (7.6)	44.7 (3.6)	47.8 (2.9)	39.1 (1.1)	47.0 (2.3)	38.2 (0.4)	52.2 (7.0)	44.3 (4.6)
S:$O_{3'}$	34.2 (−1.4)	36.6 (−4.5)	40.8 (−4.1)	32.5 (−5.5)	39.9 (−4.8)	31.5 (−6.3)	42.5 (−2.7)	35.8 (−3.9)
S:$O_{5'}$	39.6 (4.0)	36.4 (−4.7)	44.3 (−0.6)	28.5 (−9.5)	43.0 (−1.7)	27.3 (−10.5)	50.3 (5.1)	34.2 (−5.5)
S:$O_{2'}$	34.9 (−0.7)	38.3 (−2.8)	41.8 (−3.1)	32.3 (−5.7)	40.9 (−3.8)	31.1 (−6.7)	43.8 (−1.4)	39.1 (−0.6)

[a] Relative free energy values (kcal/mol) in the gas phase ($\Delta G^{\ddagger}$) and in solution ($\Delta G^{\ddagger}_{aq}$) for the rate-controlling transition state of the forward (fwd) monoanionic reaction (i.e., relative to the reactants at infinite separation), and of the reverse (rev) monoanionic reaction (i.e., relative to the product state). Shown in parentheses are the relative free energy differences ($\Delta\Delta G^{\ddagger}$ and $\Delta\Delta G^{\ddagger}_{aq}$) with respect to the native reaction.

3′ position provides the largest barrier relaxation relative to the native reaction (−1.4 kcal/mol for the methanolysis reaction and −4.5 kcal/mol for transesterification).

Substitution at the nucleophile/leaving group positions for the monoanionic reactions are affected mainly by two factors. On one hand, thiols are poorer nucleophiles in attack to phosphate centers and better leaving groups than alcohols. On the other hand, because thiols are more acidic than alcohols (in both the gas phase and in solution), they are less prone to receive a proton as a leaving group and more prone to donate it when acting as nucleophile. These two effects partially counterbalance one another, and hence, thio substitutions at the 2′ and 5′ positions lead to only a moderate change in the gas-phase free energy barriers compared to thio effects in the dianionic mechanisms. Thio substitution at $O_{5'}$ leads to a higher monoanionic barrier for methanolysis (4.0 kcal/mol) and a lower barrier for transesterification (−4.7 kcal/mol). Thio substitution at the $O_{2'}$ oxygen leads to only a slight change in the monoanionic gas-phase free energy barrier for methanolysis (−0.7 kcal/mol) and a moderate acceleration for transesterification (−2.8 kcal/mol) relative to the native reaction.

Monoanionic Reactions in Solution. Solvent effects have a significant effect on the monoanionic reaction barriers, as discussed in Section 3.2.3, although not nearly as large as for the dianionic reactions. Overall, solvent effects tend to increase the monoanionic free energy barriers for the forward methanolysis reactions and decrease the barriers for the reverse transesterification reactions relative to those in the gas phase. This is because solvation preferentially stabilizes the reactant state, where the neutral nucleophile and monoanionic phosphate/phosphorothioate substrate are infinitely separated. The smaller monoanionic substrate is more highly solvated than in the transition state or reactive intermediates (see Table 4). In general, thio substitution leads to lower solvation free energy values, and hence the aqueous free energy barrier for the native methanolysis reaction is raised the most with respect to the gas-phase reactions.

The overall picture that emerges for the monoanionic reactions when solvent contributions are considered is that thio substitution at the nonbridging positions generally increases only moderately the barriers for in-line methanolysis and transesterification reactions. Thio substitution at the 3′ position leads to a significant barrier relaxation for both methanolysis (−4.1 kcal/mol) and transesterification (−5.5 kcal/mol) with the PCM model. Thio substitution at the 2′ and 5′ positions reduces the barriers for both monoanionic methanolysis and transesterification reactions with both the PCM and CPCM solvation models. Of these, the smallest predicted barrier relaxation is for the S:$O_{5'}$ forward methanolysis reaction (−0.6 kcal/mol), and the largest predicted barrier relaxation is for the S:$O_{5'}$ transesterification reaction (−9.5 kcal/mol). The SM5 model follows the same general trends as the PCM and CPCM models, except that the SM5 model predicts the S:$O_{5'}$ reaction to have a substantially increased methanolysis barrier relative to the native reaction by 5.1 kcal/mol.

4.3. Comparison of Dianionic and Monoanionic Reactions in Solution. The rate-controlling aqueous free energy barriers for (forward) methanolysis and (reverse) transesterification reactions calculated with the PCM, CPCM, and SM5 models are shown in Tables 6 and 7. The PCM model predicts very similar values and identical trends to the CPCM model. The SM5 model, on the other hand, exhibits some significant differences, in particular, considerably lower aqueous free energy barriers for the dianionic reactions, in many cases by 15 kcal/mol or more. Unless otherwise stated, reference to explicit aqueous free energy values in this subsection will correspond to those calculated with the PCM solvation model.

4.3.1. Methanolysis Barriers. The dianionic native reaction has a forward methanolysis rate-controlling aqueous free energy barrier of 41.1 kcal/mol that is 3.8 kcal/mol lower than that of the monoanionic native reaction. In fact, the rate-controlling aqueous free energy barriers for methanolysis are lower for all the dianionic reactions, with the exception of the S:$O_{5'}$ and S:$O_{2'}$ reactions that are predicted to be 11.6 and 0.6 kcal/mol lower, respectively, for the monoanionic reaction.

Thio substitutions at the nonbridging positions have a small thio effect (between −0.5 and 0.5 kcal/mol) for the dianionic methanolysis reaction, whereas they have a moderate thio effect (between 2.1 and 2.9 kcal/mol) for the monoanionic reaction. Substitution at the 3′ position has a similar moderate thio effect for both the dianionic (−4.8 kcal/mol) and monoanionic (−4.1 kcal/mol) methanolysis. The S:$O_{5'}$ reaction has the largest thio effect (14.8 kcal/mol) of the dianionic reactions, whereas it has the smallest thio effect (−0.6 kcal/mol) for the monoanionic reactions. This arises because of the replacement of the methoxide nucleophile with methanethiolate. Thiolates, although proficient enhanced leaving groups, have been demonstrated to be particularly reticent toward nucleophilic attack to phosphate centers[98] (see below for a discussion of comparison with experiment). The S:$O_{2'}$ methanolysis reaction exhibits a relatively moderate thio effect that changes sign from 1.3 kcal/mol for the dianionic reaction to −3.1 kcal/mol for the monoanionic reaction.

4.3.2. Transesterification Barriers. The monoanionic native reaction has a reverse transesterification rate-controlling aqueous free energy barrier of 28.3 kcal/mol that is 9.7 kcal/mol lower than that of the monoanionic native reaction. All of the dianionic transesterification reactions have lower barriers than the cor-

responding monoanionic reactions, with the exception of the S:$O_{2'}$ reaction; the smallest difference occurs for the S:$O_{5'}$ reaction (6.7 kcal/mol) and the largest occurs for the S:$O_{2'}$ reaction (−18.9 kcal/mol).

All of the dianionic transesterification thio effects involve barrier relaxation (lower barriers relative to that of the native reaction). with the exception of the 2′ thio substitution that results in a 22.9 kcal/mol barrier elevation. This arises, as for the 5′ thio substitution in the dianionic methanolysis reaction, by the replacement of an alkoxide nucleophile by the corresponding thiolate. In striking contrast to the dianionic case, the monoanionic S:$O_{2'}$ transesterification results in barrier relaxation of −5.7 kcal/mol. Thio substitutions at the nonbridging positions lead to mild barrier relaxation (between −0.8 and −1.6 kcal/mol) for dianionic transesterification and barrier elevation (between 1.1 and 1.8 kcal/mol) for the monoanionic reactions. As for the methanolysis reaction, the 3′ thio substitutions lead to fairly significant barrier relaxation that are similar in the dianionic (−4.9 kcal/mol) and monoanionic (−5.5 kcal/mol) transesterification reactions. The largest barrier relaxation occurs for the S:$O_{5'}$ transesterification for both the dianionic (−6.5 kcal/mol) and monoanionic (−9.5 kcal/mol) reactions.

A comparison of the thio effects for the nucleophilic and leaving group positions underscore the balance between acidity/basicity and nucleophilic/leaving group character. In the case of the dianionic reactions, the main effect on the barriers is governed by the enhanced leaving group capacity and poorer phosphate nucleophilicity of thiolates relative to the corresponding alkoxides. However, in the monoanionic reactions, this effect is counterbalanced by the increased acidity of thiols relative to the corresponding alcohols that lowers the barrier to nucleophilic activation by deprotonation or stabilizes the leaving group by hydrogen bonding and subsequent protonation.

4.4. Comparison with Experiment. A multitude of experiments on thio effects on the hydrolysis of RNA-type nucleotides have been reported in the literature.[15,16] Sulfur substitution can affect all steps of the hydrolytic mechanism, and therefore, the measured changes on the overall reaction rates may not yield to simple interpretation. In the case of alkaline hydrolysis of RNA, it is reasonably well established that the mechanism is a two-step in-line process that proceeds through a pentacoordinate phosphorane transition state with inversion of the phosphate center. The first step is that of transesterification (Scheme 1) that produces a 2′,3′ cyclic phosphate, followed by a subsequent second hydrolysis step that leads to a hydrolyzed 3′ phosphate. Hydrolysis of RNA under neutral and acid pH, however, is more complicated. Along with transesterification and hydrolytic steps, there can be other types of steps involved in the mechanism, such as pseudorotation, migration, and in the case of thio substitution, desulfurization.[15,16] These steps will be a topic of future work. In the present work, discussion will focus mainly on the comparison of experimental data of thio effects under alkaline conditions, corresponding to the calculated dianionic reaction models. Unless otherwise stated, reference to explicit aqueous free energy values in this subsection will correspond to those calculated with the PCM solvation model.

The general picture that emerges from kinetic experiments is that hydrolysis of RNA is most sensitive to thio substitutions at the nucleophile/leaving group positions (5′/2′). Hydrolysis is only moderately sensitive to sulfur substitution at the nonbridging positions. Thio substitution at the 3′ position leads to a significant rate acceleration. All of these experimental observations are influenced by different experimental conditions, including pH, solvent, and ionic strength, and can vary between specific nucleotide sequences.

4.4.1. Substitutions at the Nucleophilic and Leaving Group Positions (5′/2′). The transesterification of 5′-phosphorothioates[99,100] is 4−5 orders of magnitude faster than the corresponding native reaction at alkali pH. This corresponds to a difference in reaction barriers of roughly 5−7 kcal/mol. The PCM value for barrier relaxation in the S:$O_{5'}$ reaction (−6.5 kcal/mol) is in very good agreement.

On the other hand, transesterification of 2′ thiosubstituted phosphates has been observed to be only possible when strongly electronegative groups are present as the leaving group.[16] In these cases, the reaction rate is considerably slower than that of the native reaction at alkaline pH. Dantzman et al.[98] reported that the rate of the thiolate attack on the adjacent phosphodiester bond is 10^7-fold slower than that of the corresponding alkoxide for the transesterification reaction of 2′-deoxy-2′-thiouridine 3′-(*p*-nitrophenyl phosphate), corresponding to a roughly 10 kcal/mol difference in free energy. This is in qualitative agreement with the high increase in barrier (Table 6) for the dianionic reaction upon 2′ thio substitution (22.9 kcal/mol). The rate deceleration under neutral pH is reduced to 27-fold (roughly 2 kcal/mol in free energy difference). The present calculations predict a moderate barrier relaxation for the monoanionic reaction (−5.7 kcal/mol). As mentioned previously, the reaction under neutral pH is likely not that of the simple monoanionic reaction model considered here, but is significantly more complicated and likely to involve explicit water molecules.

4.4.2. Substitution at the Nonbridging Positions (O_{P1},O_{P2}). Experimental studies of thio effects at the nonbridging phosphoryl oxygen positions provides a useful mechanistic probe into enzymatic and nonenzymatic RNA hydrolysis and the role of metal binding. Single thio substitution at the nonbridging positions have been reported to have almost no effect on the alkaline cleavage rate for various dinucleotides.[21,101−106] For instance, in the case of 3′,5′-Up(s)U, Almer et al.[102,103] reported ratios of rate constants *k*(phosphate)/*k*(thiophosphate) of 1.3 and 0.78 at the R_P and S_P positions, respectively. Oivanen et al.[107] also found a negligible kinetic thio effect for the alkaline hydrolysis of 3′,5′-UpU. In agreement with these experimental findings, the results in Table 6 point to only very moderate thio effects for the alkaline transesterification (−1.6 kcal/mol) and methanolysis (−0.5 kcal/mol) for the S:O_{P1} reaction. On the other hand, the effect of double thio substitution at the nonbridging positions is more controversial. Nielsen et al.[108,109] observed a higher chemical and enzymatic stability for the phosphorodithioate linkage in RNA as compared to natural RNA. More recently, however, Ora et al.[106] determined that replacement of the remaining nonbridging oxygen of phosphoromonothioates with sulfur has a surprisingly small effect on the kinetics of hydrolysis and transesterification at alkaline pH. The present calculations support the latter data. The aqueous free energy barriers for dianionic S:O_{P1},O_{P2} methanolysis and transesterification are predicted to undergo only very moderate elevation and relaxation, respectively (0.5 and −0.8 kcal/mol, respectively). These results are somewhat in contradiction to those of a recent QM/MM study of dianionic transesterification thio effects with a semiempirical Hamiltonian[95,96] that predicted significantly elevated barriers for single and double thio substitutions. The origin of these differences likely resides mainly in the choice of nonbonded QM/MM van der Waals parameters, a more rigorous parametrization for which is a focus of current efforts. Nonetheless, the quantitative understanding

of single and double thio substitutions for model reactions remains only partially understood.

Under neutral and acidic conditions, the interpretation of experimental results is more controversial due to the fact that desulfurization effectively competes with the rupture of P−OR bonds (R = alkyl group). This suggests that thiophosphorane monoanionic intermediates are sufficiently long-lived to allow pseudorotation.[54,68] As characterized by the free energy profiles of Figures 1, 2, and 3, thio substitution at the nonbridging positions, rather than stabilizing the thiophosphorane intermediate structures, increases the barrier for endocyclic cleavage, resulting effectively in a longer-lived intermediate than in the native reaction. Regarding the kinetic rates, thio substitution appears to accelerate[16,107] the departure of the 5′-linked nucleoside, but retards isomerization via pseudorotation. The thio effects observed in this work for monoanionic in-line transesterification and methanolysis indicate a moderate increase in these barriers. As in the dianionic case, double thio substitution in the monoanionic reaction leads to very similar aqueous free energy barriers to that of the native reaction, and is consistent with the suggestion that single and double thio substitution at the nonbridging phosphoryl positions lead to small thio effects in nonenzymatic models.

4.4.3. Substitution at the 3′ Position. Thio effects at the 3′ position have been the focus of several experimental studies[15,16] due to the origin of the moderate reaction rate acceleration that is produced. Base-catalyzed cleavage of the thiomodified RNA, for instance, is 200−2000-fold faster than the native reaction.[85] This corresponds to an aqueous free energy barrier relaxation of 3−4.5 kcal/mol relative to the native reaction. The calculated barrier relaxation for dianionic transesterification (−4.9, −3.7, and −3.4 kcal/mol with the PCM, CPCM, and SM5 solvation models, respectively) are in good agreement with this estimated experimental barrier relaxation. A similar barrier relaxation is predicted for the in-line monoanionic transesterification. However, under acidic conditions, the experimental thio effect is close to unity.[85] As mentioned previously, the monoanionic mechanism is likely more complex than the reaction model presented here. Nonetheless, the monoanionic reaction model serves as a useful benchmark that provides qualitative insight into mechanism and marks an upper bound to the expected barriers under acidic conditions.

4.5. Limitations of the Current Approach. A major objective in the design of theoretical methods for RNA catalysis is to provide accurate simulation models for phosphoryl transfer reactions that are able to reproduce known experimental observables such as rate constants, kinetic, and equilibrium isotope and thio effects. The resulting theoretical calculations may aid in the interpretation of experiments as well as be applied in a predictive capacity to systems where limited experimental data is available. Toward this end, it is important to assess the limitations of theoretical methods and identify directions for future improvement.

The main sources of error in the present work include: (1) Errors introduced by limitations of the electronic structure methods. (2) Errors introduced by inadequacy in the treatment of solvation. (3) Errors introduced by approximations in the calculation of the free energy. (4) Errors introduced by incomplete exploration of alternate mechanistic pathways.

The above list is, of course, subjective, in that all of the items are coupled. The first item regards the errors in the density functional method itself. It is known that density functional theory with the local density, gradient corrected, and many hybrid exchange correlation functionals systematically underestimate reaction barriers,[110] although improved density functional models for thermochemistry and chemical kinetics continue to emerge.[110] In the present case, comparison with MP2 calculations and other electronic structure methods suggest the errors to be on the order of a few kcal/mol in absolute (adiabatic) barrier heights and even smaller for comparison of relative barrier heights.

Another main source of error involves the treatment of solvation.[70] First, the neglect of solvent-induced structural relaxation is problematic, although preliminary results for the dianionic reactions indicate that inclusion solvation at the continuum level changes the activation barriers by only a few kcal/mol and increases the degree of associative character. A more serious concern involves the inability of any of the current implicit solvation models to appropriately predict relative solvation energies for multiple charge states, which is critical for reactions that involve the association (or dissociation) of charged species, such as the dianionic reactions studied here. In the present case, it is likely that the dianionic transition states are *understabilized*, leading to overpredicted activation barriers to methanolysis in solution. For example, in the dianionic mechanism of ethylene phosphate hydrolysis, the experimental free energy barriers are estimated to be on the order of 21−24 kcal/mol[38] (based on the experimental estimate of the activation free energy of 32 kcal/mol for dimethyl phosphate and the observed 10^6−10^8-fold rate acceleration for ethylene phosphate), whereas the barriers to related methanolysis reaction in the present work predict barriers for the native reaction that range between 30.2 (SM5) and 41.1 (PCM) kcal/mol. Additionally, the entropic contribution to the activation free energy, which in the current work is based on the gas-phase structures, can be a grossly inadequate assumption for the solution reactions,[111,112] especially when comparing concerted and stepwise mechanisms that may involve dissociative steps, as has been discussed in studies of reference reaction models for serine[113] and cysteine[114] proteases. This leads to the problem of inadequate exploration of alternate reaction pathways, such as the dissociative pathway.[46−48] Although the exploration of multidimensional potential energy surfaces for both the associative and dissociative paths for the series of 12 reactions is beyond the scope of the present work, it is nonetheless important to emphasize that other mechanisms are of interest and important to continue to explore and characterize.

The sources of error mentioned above could be, in principle, greatly reduced with molecular simulations using appropriate hybrid QM/MM potentials. In particular, if a sufficiently fast and accurate quantum model could be designed specifically for phosphoryl transfer reactions based on high-level quantum chemical calculations and available experiment, some of the error associated with the limitations of the density functional methods could be reduced. If QM/MM calculations were performed in a suitably accurate explicit solvation model, presumably a significantly more robust treatment of solvation would result. Use of molecular simulation to produce reaction free energy (potential of mean force) profiles would alleviate problems associated with sampling and, in particular, eliminate the large errors in the entropic component of the activation free energy. Finally, if a multidimensional mapping of the relevant reactive coordinates were made with, for example, the techniques of umbrella sampling[115] and weighted histogram analysis,[116] further exploration and characterization of alternate reaction pathways and mechanisms would be possible. The realization of these goals relies, to a large extent, on the design

of new quantum models for phosphoryl transfer reactions that are highly accurate and yet computationally tractable for use in QM/MM simulations. The calculation results presented herein serves as an important set of benchmark data for the design of these new-generation quantum models.

5. Conclusion

The present work presents results of a density functional and continuum solvation study of thio effects on the in-line mechanism of methanolysis of ethylene phosphate, a reverse reaction model for RNA transesterification. Solvation is examined with three established solvation models: PCM, CPCM, and SM5. Results for a series of 12 reactions that include the native reaction, single thio substitution at each of the distinct phosphoryl oxygen positions, and a double thio substitution at the nonbridging positions are presented. Both dianionic and monoanionic reaction models are considered, corresponding to reaction models under alkaline and nonalkaline conditions, respectively. These reactions represent an important series of chemical modifications used to probe enzyme and ribozyme mechanisms. The role of chemical modification, protonation state, and solvation are systematically examined, and extensive comparison with available experimental results are made. Together, these results provide insight into the nature of thio effects on the mechanism and rate-controlling barriers for nonenzymatic methanolysis and transesterification.

Ultimately, it is the goal of the authors to provide new-generation multiscale quantum models to study a wide range of phosphoryl transfer reactions in realistic biological environments. This goal requires the synchronous design of highly accurate quantum and solvation models, as well as models for macromolecular enzymatic environments. Toward this end, it is essential to characterize the assets and limitations of current quantum chemical and solvation models and make extensive comparisons with available experimental results. In the present work, high-level density functional calculations are tested with several implicit solvation models and compared with experiment. Arguably, the weakest link in the modeling chain at this level involves the treatment of solvation that should more realistically include participation by many more explicit solvent molecules and sampling of their relevant degrees of freedom with, for example, a linear-scaling electronic structure method or hybrid QM/MM model. However, such an approach requires a quantum method that is sufficiently fast to make these calculations tractable with reasonable computational resources. The density functional results presented here serve as an important benchmark set of high-level quantum data that can be used in the design of new semiempirical quantum models for hybrid QM/MM simulations and linear-scaling electronic structure calculations. Hence, in addition to the biological insight provided by the analysis of the present data, the comparison with experiment and assessment of the limits of the models that were employed acts as a guide in the design of new-generation multiscale models for simulations of phosphoryl transfer reactions with greater accuracy and reliability.

Acknowledgment. D.Y. is grateful for financial support provided by the National Institutes of Health (grant GM62248), and the Army High Performance Computing Research Center (AHPCRC) under the auspices of the Department of the Army, Army Research Laboratory (ARL) under Cooperative Agreement number DAAD19-01-2-0014. X.L. thanks the MSI for a Research Scholar Award, the Basque Government (Eusko Jaurlaritza), and the University of the Basque Country (Eusko Herriko Unibersitatea) for financial support. Computational resources were provided by the Minnesota Supercomputing Institute.

References and Notes

(1) Hughes, M. D.; Hussain, M.; Nawaz, Q.; Sayyed, P.; Akhtar, S. The cellular delivery of antisense oligonucleotides and ribozymes. *DDT* **2001**, *6*, 313−315.

(2) Usman, N.; Beigelman, L.; McSwiggen, J. A. Hammerhead ribozyme engineering. *Curr. Opin. Struct. Biol.* **1996**, *1*, 527−533.

(3) Uhlmann, E.; Peyman, A. Antisense oligonucleotides: a new therapeutic principle. *Chem. Rev.* **1990**, *90*, 543−584.

(4) Silverman, S. K. Rube Goldberg goes (ribo)nuclear? Molecular switches and sensors made from RNA. *RNA* **2003**, *9*, 377−383.

(5) Sekella, P. T.; Rueda, D.; Walter, N. G. A biosensor for theophylline based on fluorescence detection of ligand-induced hammerhead ribozyme cleavage. *RNA* **2002**, *8*, 1242−1252.

(6) Puerta-Fernández, E.; Romero-López, C.; Barroso-Deljesus, A.; Berzal-Herranz, A. Ribozymes: recent advances in the development of RNA tools. *FEMS Microbiol. Rev.* **2003**, *27*, 75−97.

(7) Cech, T. R. Ribozyme engineering. *Curr. Opin. Struct. Biol.* **1992**, *2*, 605−609.

(8) Breaker, R. R. In vitro selection of catalytic polynucleotides. *Chem. Rev.* **1997**, *97*, 371−390.

(9) Scott, W. G.; Klug, A. Ribozymes: structure and mechanism in RNA catalysis. *Trends Biochem. Sci.* **1996**, *21*, 220−224.

(10) Scott, W. G. RNA catalysis. *Curr. Opin. Struct. Biol.* **1998**, *8*, 720−726.

(11) Scott, W. G. RNA structure, metal ions, and catalysis. *Curr. Opin. Struct. Biol.* **2000**, *3*, 705−709.

(12) Fedor, M. J. The role of metal ions in RNA catalysis. *Curr. Opin. Struct. Biol.* **2002**, *12*, 289−295.

(13) Doherty, E. A.; Doudna, J. A. Ribozyme Structures and Mechanisms. *Annu. Rev. Biophys. Biomol. Struct.* **2001**, *30*, 457−475.

(14) Perreault, D. M.; Anslyn, E. V. Unifying the Current Data on the Mechanism of Cleavage-Transesterification of RNA. *Angew. Chem., Int. Ed. Engl.* **1997**, *36*, 432−450.

(15) Zhou, D.-M.; Taira, K. The Hydrolysis of RNA: From Theoretical Calculations to the Hammerhead Ribozyme-Mediated Cleavage of RNA. *Chem. Rev.* **1998**, *98*, 991−1026.

(16) Oivanen, M.; Kuusela, S.; Lönnberg, H. Kinetics and Mechanisms for the Cleavage and Isomerization of the Phosphodiester Bonds of RNA by Brønsted Acids and Bases. *Chem. Rev.* **1998**, *98*, 961−990.

(17) Scott, W. G.; Murray, J. B.; Arnold, J. R. P.; Stoddard, B. L.; Klug, A. Capturing the structure of a catalytic RNA intermediate: The Hammerhead Ribozyme. *Science* **1996**, *274*, 2065−2069.

(18) Scott, W. G. Biophysical and biochemical investigations of RNA catalysis in the hammerhead ribozyme. *Q. Rev. Biophys.* **1999**, *32*, 241−294.

(19) Walter, N. G.; Burke, J. M. The hairpin ribozyme: structure, assembly, and catalysis. *Curr. Opin. Chem. Biol.* **1998**, *2*, 24−30.

(20) Rupert, P. B.; Massey, A. P.; Sigurdsson, S. T.; Ferré-D'Amaré, A. R. Transition State Stabilization by a Catalytic RNA. *Science* **2002**, *298*, 1421−1424.

(21) Herschlag, D.; Piccirilli, J. A.; Cech, T. R. Ribozyme-Catalyzed and Nonenzymatic Reactions of Phosphate Effects upon Substitution of Sulfur for a Nonbridging Phosphoryl Diesters: Rate Oxygen Atom. *Biochemistry* **1991**, *30*, 4844−4854.

(22) Usman, N.; Cedergren, R. Exploiting the chemical synthesis of RNA. *Trends Biochem. Sci.* **1992**, *17*, 334−339.

(23) Catrina, I. E.; Hengge, A. C. Comparisons of phosphorothioate and phosphate monoester transfer reactions: Activation parameters, solvent effects, and the effect of metal ions. *J. Am. Chem. Soc.* **1999**, *121*, 2156−2163.

(24) Smith, J. S.; Nikonowicz, E. P. Phosphorothioate Substitution Can Substantially Alter RNA Conformation. *Biochemistry* **2000**, *39*, 5642−5652.

(25) Catrina, I. E.; Hengge, A. C. Comparisons of Phosphorothioate with Phosphate Transfer Reactions for a Monoester, Diester, and Triester: Isotope Effect Studies. *J. Am. Chem. Soc.* **2003**, *125*, 7546−7552.

(26) Breslow, R.; Chapman, W. H., Jr. On the mechanism of action of ribonuclease A: Relevance of enzymatic studies with a *p*-nitrophenyl phosphate ester and a thiophosphate ester. *Proc. Natl. Acad. Sci. U.S.A.* **1996**, *93*, 10018−10021.

(27) Åqvist, J.; Kolmodin, K.; Florian, J.; Warshel, A. Mechanistic alternatives in phosphate monoester hydrolysis: what conclusions can be drawn from avaliable experimental data? *Chem. Biol.* **1999**, *6*, R71−R80.

(28) Warshel, A. *Computer Modeling of Chemical Reactions in Enzymes and Solutions*; John Wiley and Sons: New York, 1991.

(29) Karplus, M. Aspects of Protein Reaction Dynamics: Deviations from Simple Behavior. *J. Phys. Chem. B* **2000**, *104*, 11−27.

(30) Friesner, R. A.; Beachy, M. D. Quantum mechanical calculations on biological systems. *Curr. Opin. Struct. Biol.* **1998**, *8*, 257−262.

(31) Warshel, A. Computer simulations of enzyme catalysis: methods, progress, and insights. *Annu. Rev. Biophys. Biomol. Struct.* **2003**, *32*, 425−443.

(32) Lim, C.; Karplus, M. Nonexistence of dianionic pentacovalent intermediates in an ab initio study of the base-catalysed hydrolysis of ethylene phosphate. *J. Am. Chem. Soc.* **1990**, *112*, 5872−5873.

(33) Uchimaru, T.; Tanabe, K.; Nishikawa, S.; Taira, K. Ab Initio Studies of a Marginally Stable Intermediate in the Base-Catalyzed Methanolysis of Dimethyl Phosphate and Nonexistence of the Stereoelectronically Unfavorable Transition State. *J. Am. Chem. Soc.* **1991**, *113*, 4351−4353.

(34) Lim, C.; Tole, P. Concerted Hydroxyl Ion Attack and Pseudorotation in the Base-Catalyzed Hydrolysis of Methyl Ethylene Phosphate. *J. Phys. Chem.* **1992**, *96*, 5217−5219.

(35) Mercero, J. M.; Barrett, P.; Lam, C. W.; Fowler, J. E.; Ugalde, J. M.; Pedersen, L. G. Quantum Mechanical Calculations on Phosphate Hydrolysis Reactions. *J. Comput. Chem.* **2000**, *21*, 43−51.

(36) Arantes, G. M.; Chaimovich, B. Thiolysis and Alcoholysis of Phosphate Tri- and Monoesters with Alkyl and Aryl Leaving Groups. An ab Initio Study in the Gas Phase. *J. Phys. Chem. A* **2005**, *109*, 5625−5635.

(37) Dejaegere, A.; Lim, C.; Karplus, M. Dianionic Pentacoordinate Species in the Base-Catalyzed Hydrolysis of Ethylene and Dimethyl Phosphate. *J. Am. Chem. Soc.* **1991**, *113*, 4353−4355.

(38) Dejaegere, A.; Karplus, M. Hydrolysis Rate Difference between Cyclic and Acyclic Phosphate Esters: Solvation versus Strain. *J. Am. Chem. Soc.* **1993**, *115*, 5316−5317.

(39) Tole, P.; Lim, C. New Insights into the Base-Catalyzed Hydrolysis of Methyl Ethylene Phosphate. *J. Phys. Chem.* **1993**, *97*, 6212−6219.

(40) Tole, P.; Lim, C. The Significance of Electrostatic Effects in Phospho-Ester Hydrolysis. *J. Am. Chem. Soc.* **1994**, *116*, 3922−3931.

(41) Chang, N.; Lim, C. An ab initio study of nucleophilic attack of trimethyl phosphate: Factors influencing site reactivity. *J. Phys. Chem. A* **1997**, *101*, 8706−8713.

(42) Lopez, X.; Dejaegere, A.; Karplus, M. Solvent Effects on the Reaction Coordinate of the Hydrolysis of Phosphates and Sulfates: Application of Hammond and Anti-Hammond Postulates to Understand Hydrolysis in Solution. *J. Am. Chem. Soc.* **2001**, *123*, 11755−11763.

(43) Lopez, X.; Schaefer, M.; Dejaegere, A.; Karplus, M. Theoretical evaluation of pK_a in phosphoranes: implications for phosphate ester hydrolysis. *J. Am. Chem. Soc.* **2002**, *124*, 5010−5018.

(44) Chen, X.; Zhan, C.-G. Theoretical determination of activation free energies for alkaline hydrolysis of cyclic and acyclic phosphodiesters in aqueous solution. *J. Phys. Chem. A* **2004**, *108*, 6407−6413.

(45) Xu, D.; Guo, H.; Liu, Y.; York, D. M. Theoretical Studies of Dissociative Phosphoryl Transfer in Interconversion of Phosphoenolpyruvate to Phosphonopyruvate: Solvent Effects, Thio Effects, and Implications for Enzymatic Reactions. *J. Phys. Chem. B* **2005**, *109*, 13827−13834.

(46) Florián, J.; Warshel, A. A fundamental assumption about OH-attack in phosphate ester hydrolysis is not fully justified. *J. Am. Chem. Soc.* **1997**, *119*, 5473−5474.

(47) Florián, J.; Warshel, A. Phosphate ester hydrolysis in aqueous solution: Associative versus dissociative mechanisms. *J. Phys. Chem. B* **1998**, *102*, 719−734.

(48) Hu, C.-H.; Brinck, T. Theoretical Studies of the Hydrolysis of the Methyl Phosphate Anion. *J. Phys. Chem. A* **1999**, *103*, 5379−5386.

(49) Glennon, T. M.; Warshel, A. Energetics of the catalytic reaction of Ribonuclease A: A computational study of alternative mechanisms. *J. Am. Chem. Soc.* **1998**, *120*, 10234−10247.

(50) Jones, G. A.; Carpenter, B. K.; Paddon−Row, M. N. Application of Trajectory Surface Hopping to the Study of Intramolecular Electron Transfer in Polyatomic Organic Systems. *J. Am. Chem. Soc.* **1998**, *120*, 5488−5498.

(51) Lopez, X.; York, D. M.; Dejaegere, A.; Karplus, M. Theoretical Studies on the Hydrolysis of Phosphate Diesters in the Gas Phase, Solution, and RNase A. *Int. J. Quantum Chem.* **2002**, *86*, 10−26.

(52) Liang, C.; Allen, L. C. Sulfur Does Not Form Double Bonds in Phosphorothioate Anions. *J. Am. Chem. Soc.* **1987**, *109*, 6449−6453.

(53) Florián, J.; Štrajbl, M.; Warshel, A. Conformational flexibility of phosphate, phosphonate, and phosphorothioate methyl esters in aqueous solution. *J. Am. Chem. Soc.* **1998**, *120*, 7959−7966.

(54) López, C. S.; Faza, O. N.; Gregersen, B. A.; Lopez, X.; De Lera, A. R.; York, D. M. Pseudorotation of Natural and Chemically Modified Biological Phosphoranes: Implications for RNA Catalysis. *Chem. Phys. Chem.* **2004**, *5*, 1045−1049.

(55) Liu, Y.; Lopez, X.; York, D. M. Kinetic isotope effects on thiosubstituted biological phosphoryl transfer reactions from density functional theory. *Chem. Commun.* **2005**, *31*, 3909−3911.

(56) Uchimaru, T.; Stec, W. J.; Taira, K. Mechanism of the Chemoselective and Stereoselective Ring Opening of Oxathiaphospholanes: An Ab Initio Study. *J. Org. Chem.* **1997**, *62*, 5793−5800.

(57) Uchimaru, T.; Stec, W. J.; Tsuzuki, S.; Hirose, T.; Tanabe, K.; Taira, K. Ab initio investigation on nucleophilic ring opening of 1,3,2-oxathiaphospholane: nucleophilic substitution at phosphorus coupled with pseudorotation. *Chem. Phys. Lett.* **1996**, *263*, 691−696.

(58) Becke, A. D. Density functional exchange-energy approximation with correct asymptotic behavior. *Phys. Rev. A.* **1988**, *38*, 3098−3100.

(59) Becke, A. D. Density functional thermochemistry. III. The role of exact exchange. *J. Chem. Phys.* **1993**, *98*, 5648−5652.

(60) Lee, C.; Yang, W.; Parr, R. G. Development of the Colle−Savetti Correlation energy formula into a functional of the electron density. *Phys. Rev. B.* **1988**, *37*, 785−789.

(61) Peng, C.; Ayala, P. Y.; Schlegel, H. B.; Frisch, M. J. Using redundant internal coordinates to optimize equilibrium geometries and transition states. *J. Comput. Chem.* **1996**, *17*, 49−56.

(62) Bauernschmitt, R.; Ahlrichs, R. Stability analysis for solutions of the closed-shell Kohn−Sham equation. *J. Chem. Phys.* **1996**, *104*, 9047−9052.

(63) Seeger, R.; Pople, J. A. Self-consistent molecular orbital methods. XVIII. Constraints and stability in Hartree−Fock theory. *J. Chem. Phys.* **1977**, *66*, 3045−3050.

(64) ×aeFrisch, Æ.; Frisch, M. J. *Gaussian 98 User's Reference*, 2nd ed.; Gaussian, Inc.: Pittsburgh, PA, 1999.

(65) Frisch, M. J.; Trucks, G. W.; Schlegel, H. B.; Scuseria, G. E.; Robb, M. A.; Cheeseman, J. R.; Montgomery, J. A., Jr.; Vreven, T.; Kudin, K. N.; Burant, J. C.; Millam, J. M.; Iyengar, S. S.; Tomasi, J.; Barone, V.; Mennucci, B.; Cossi, M.; Scalmani, G.; Rega, N.; Petersson, G. A.; Nakatsuji, H.; Hada, M.; Ehara, M.; Toyota, K.; Fukuda, R.; Hasegawa, J.; Ishida, M.; Nakajima, T.; Honda, Y.; Kitao, O.; Nakai, H.; Klene, M.; Li, X.; Knox, J. E.; Hratchian, H. P.; Cross, J. B.; Bakken, V.; Adamo, C.; Jaramillo, J.; Gomperts, R.; Stratmann, R. E.; Yazyev, O.; Austin, A. J.; Cammi, R.; Pomelli, C.; Ochterski, J. W.; Ayala, P. Y.; Morokuma, K.; Voth, G. A.; Salvador, P.; Dannenberg, J. J.; Zakrzewski, V. G.; Dapprich, S.; Daniels, A. D.; Strain, M. C.; Farkas, O.; Malick, D. K.; Rabuck, A. D.; Raghavachari, K.; Foresman, J. B.; Ortiz, J. V.; Cui, Q.; Baboul, A. G.; Clifford, S.; Cioslowski, J.; Stefanov, B. B.; Liu, G.; Liashenko, A.; Piskorz, P.; Komaromi, I.; Martin, R. L.; Fox, D. J.; Keith, T.; Al-Laham, M. A.; Peng, C. Y.; Nanayakkara, A.; Challacombe, M.; Gill, P. M. W.; Johnson, B.; Chen, W.; Wong, M. W.; Gonzalez, C.; Pople, J. A. *Gaussian 03*, revision B.01; Gaussian, Inc.: Wallingford, CT, 2004.

(66) Range, K.; McGrath, M. J.; Lopez, X.; York, D. M. The Structure and Stability of Biological Metaphosphate, Phosphate, and Phosphorane Compounds in the Gas Phase and in Solution. *J. Am. Chem. Soc.* **2004**, *126*, 1654−1665.

(67) Mayaan, E.; Range, K.; York, D. M. Structure and binding of Mg-(II) ions and dimetal bridge complexes with biological phosphates and phosphoranes. *J. Biol. Inorg. Chem.* **2004**, *9*, 807−817.

(68) López, C. S.; Faza, O. N.; R. De Lera, A.; York, D. M. Pseudorotation Barriers of Biological Oxyphosphoranes: A Challenge for Simulations of Ribozyme Catalysis. *Chem.−Eur. J.* **2005**, *11*, 2081−2093.

(69) Cramer, C. J. *Essentials of Computational Chemistry: Theories and Models*, 2nd ed.; John Wiley & Sons: Chichester, U.K., 2002.

(70) Cramer, C. J.; Truhlar, D. G. Implicit solvation models: equilibria, structure, spectra, and dynamics. *Chem. Rev.* **1999**, *99*, 2161−2200.

(71) Tomasi, J.; Persico, M. Molecular interaction in solution: An overview of methods based on continuous distributions of the solvent. *Chem. Rev.* **1994**, *94*, 2027−2094.

(72) Mineva, T.; Russo, N.; Sicilia, E. Solvation Effects on Reaction Profiles by the Polarizable Continuum Model Coupled with the Gaussian Density Functional Method. *J. Comput. Chem.* **1998**, *19*, 290−299.

(73) Cossi, M.; Scalmani, G.; Rega, N.; Barone, V. New developments in the polarizable continuum model for quantum mechanical and classical calculations on molecules in solution. *J. Chem. Phys.* **2002**, *117*, 43−54.

(74) Klamt, A.; Schüürmann, G. Cosmo: a new approach to dielectric screening in solvents with explicit expressions for the screening energy and its gradient. *J. Chem. Soc., Perkin Trans. 2* **1993**, *2*, 799−805.

(75) Klamt, A.; Jonas, V.; Bürger, T.; Lohrenz, J. C. W. Refinement and Parametrization of COSMO−RS. *J. Phys. Chem. A* **1998**, *102*, 5074−5085.

(76) Barone, V.; Cossi, M. Quantum Calculation of Molecular Energies and Energy Gradients in Solution by a Conductor Solvent Model. *J. Phys. Chem. A* **1998**, *102*, 1995−2001.

(77) Li, J.; Zhu, T.; Hawkins, G. D.; Winget, P.; Liotard, D. A.; Cramer, C. J.; Truhlar, D. G. Extension of the platform of applicability of the SM5.42R universal solvation model. *Theor. Chem. Acc.* **1999**, *103*, 9−63.

(78) Xidos, J. D.; Li, J.; Thompson, J. D.; Hawkins, G. D.; Winget, P. D.; Zhu, T.; Rinaldi, D.; Liotard, D. A.; Cramer, C. J.; Truhlar, D. G.; Frisch, M. J. *MN-GSM*, version 1.8; University of Minnesota: Minneapolis, MN, 2001.

(79) York, D. M.; Karplus, M. A smooth solvation potential based on the Conductor-Like Screening Model. *J. Phys. Chem. A* **1999**, *103*, 11060−11079.

(80) Khandogin, J.; Gregersen, B. A.; Thiel, W.; York, D. M. Smooth Solvation Method for d-Orbital Semiempirical Calculations of Biological Reactions. 1. Implementation. *J. Phys. Chem. B* **2005**, *109*, 9799−9809.

(81) Gregersen, B. A.; Khandogin, J.; Thiel, W.; York, D. M. Smooth Solvation Method for d-Orbital Semiempirical Calculations of Biological Reactions. 2. Application to Transphosphorylation Thio Effects in Solution. *J. Phys. Chem. B* **2005**, *109*, 9810−9817.

(82) Barone, V.; Cossi, M.; Tomasi, J. A new definition of cavities for the computation of solvation free energies by the polarizable contiuum model. *J. Chem. Phys.* **1997**, *107*, 3210−3221.

(83) Easton, R. E.; Giesen, D. J.; Welch, A.; Cramer, C. J.; Truhlar, D. G. The MIDI! basis set for quantum mechanical calculations of molecular geometries and partial charges. *Theor. Chem. Acc.* **1996**, *93*, 281−301.

(84) Liu, X.; Reese, C. B. 3′-Thiouridylyl-(3′ → 5′)-uridine. *Tetrahedron Lett.* **1996**, *37*, 925−928.

(85) Weinstein, L. B.; Earnshaw, D. J.; Cosstick, R.; Cech, T. R. Synthesis and characterization of an RNA dinucleotide containing a 3′-S-phosphorothiolate linkage. *J. Am. Chem. Soc.* **1996**, *118*, 10341−10350.

(86) Hammond, G. S. A Correlation of Reaction Rates. *J. Am. Chem. Soc.* **1955**, *77*, 334−338.

(87) Jencks, W. P. A Primer for the Bema Hapothle. An Empirical Approach to the Characterization of Changing Transition State Structures. *Chem. Rev.* **1985**, *85*, 511−527.

(88) Lide, D. R., Ed. *CRC Handbook of Chemistry and Physics*, 83rd ed.; CRC Press LLC: Boca Raton, FL, 2003.

(89) Guthrie, R. D.; Jencks, W. P. IUPAC Recommendations for the Representation of Reaction Mechanisms. *Acc. Chem. Res.* **1989**, *22*, 343−349.

(90) Pearson, R. C. Ionization Potentials and Electron Affinities in Aqueous Solution. *J. Am. Chem. Soc.* **1986**, *108*, 6109−6114.

(91) Florián, J.; Warshel, A. Langevin Dipoles Model for Ab Initio Calculations of Chemical Processes in Solution: Parametrization and Application to Hydration Free Energies of of Neutral and Ionic Solutes and Conformational Analysis in Aqueous Solutions. *J. Phys. Chem. B* **1997**, *101*, 5583−5595.

(92) Klicić, J. J.; Friesner, R. A.; Liu, S.-Y.; Guida, W. C. Accurate Prediction of Acidity Constants in Aqueous Solution via Density Functional Theory and Self-Consistent Reaction Field Methods. *J. Phys. Chem. A* **2002**, *106*, 1327−1335.

(93) Thompson, J. D.; Cramer, C. J.; Truhlar, D. G. New Universal Solvation Model and Comparison of the Accuracy of the SM5.42R, SM5.43R, C-PCM, D-PCM, and IEF−PCM Continuum Solvation Models for Aqueous and Organic Solvation Free Energies and for Vapor Pressures. *J. Phys. Chem. A.* **2004**, *108*, 6532−6542.

(94) Li, Y.; Breaker, R. R. Kinetics of RNA Degradation by Specific Base Catalysis of Transesterification Involving the 2′-Hydroxyl Group. *J. Am. Chem. Soc.* **1999**, *121*, 5364−5372.

(95) Gregersen, B. A.; Lopez, X.; York, D. M. Hybrid QM/MM study of thio effects in transphosphorylation reactions. *J. Am. Chem. Soc.* **2003**, *125*, 7178−7179.

(96) Gregersen, B. A.; Lopez, X.; York, D. M. Hybrid QM/MM Study of Thio Effects in Transphosphorylation Reactions: The Role of Solvation. *J. Am. Chem. Soc.* **2004**, *126*, 7504−7513.

(97) Foloppe, N.; Mackerell, Jr., A. D. All-atom empirical force field for nucleic acids: I. Parameter optimization based on small molecule and condensed phase macromolecular target data. *J. Comput. Chem.* **2000**, *21*, 86−104.

(98) Dantzman, C. L.; Kiessling, L. L. Reactivity of a 2′-thio nucleotide analogue. *J. Am. Chem. Soc.* **1996**, *118*, 11715−11719.

(99) Liu, X.; Reese, C. B. Uridylyl-(3′ → 5′)−(5′-thiouridine). An exceptionally base-labile diribonucleoside phosphate analogue. *Tetrahedron Lett.* **1995**, *36*, 3413−3416.

(100) Thomson, J. B.; Patel, B. K.; Jiménez, V.; Eckart, K.; Eckstein, F. Synthesis and properties of diuridine phosphate analogues containing thio and amino modifications. *J. Org. Chem.* **1996**, *61*, 6273−6281.

(101) Burgers, P. M. J.; Eckstein, F. Diastereomers of 5′-O-Adenosyl 3′-O-Uridyl Phosphorothioate: Chemical Synthesis and Enzymatic Properties. *Biochemistry* **1979**, *18*, 592−596.

(102) Almer, H.; Strömberg, R. Intramolecular transesterification in thiophosphate-analogues of an RNA-dimer. *Tetrahedron Lett.* **1991**, *32*, 3723−3726.

(103) Almer, H.; Strömberg, R. Base catalysis and leaving group dependence in intramolecular alcoholysis of uridine 3′-(aryl phosphorothioate)s. *J. Am. Chem. Soc.* **1996**, *118*, 7921−7928.

(104) Ora, M.; Oivanen, M.; Lönnberg, H. Hydrolysis and Desulfurization of the Diastereomeric Phosphoromonothioate Analogues of Uridine 2′, 3′-Cyclic Monophosphate. *J. Org. Chem.* **1996**, *61*, 3951−3955.

(105) Ora, M.; Oivanen, M.; Lönnberg, H. Phosphoester Hydrolysis and Intramolecular Transesterification of Ribonucleoside 2′- and 3′-Phosphoromonothioate Triesters: Kinetics and Mechanisms for the Reactions of 5′-O-Methyluridine 2′- and 3′-Dimethylphosphoromonothioates. *J. Org. Chem.* **1997**, *62*, 3246−3253.

(106) Ora, M.; Järvi, J.; Oivanen, M.; Lönnberg, H. Hydrolytic Reactions of the Phosphorodithioate Analogue of Uridylyl(3′,5′)uridine: Kinetics and Mechanisms for the Cleavage, Desulfurization, and Isomerization of the Internucleosidic Linkage. *J. Org. Chem.* **2000**, *65*, 2651−2657.

(107) Oivanen, M.; Ora, M.; Almer, H.; Strömberg, R.; Lönnberg H. Hydrolytic reactions of the diastereomeric phosphoromonothioate analogues of uridylyl(3′,5′)uridine: kinetics and mechanisms for desulfurization, phosphoester hydrolysis, and transesterification to the 2′,5′-isomers. *J. Org. Chem.* **1995**, *60*, 5620−5627.

(108) Nielsen, J.; Brill, W. K.-D.; Caruthers, M. H. Synthesis and characterization of dinucleoside phosphorodithioates. *Tetrahedron Lett.* **1988**, *29*, 2911−2914.

(109) Petersen, K. H.; Nielsen, J. Chemical synthesis of dimer ribonucleotides containing internucleotidic phosphorodithioate linkages. *Tetrahedron Lett.* **1990**, *31*, 911−914.

(110) Zhao, Y.; González-García, N.; Truhlar, D. G. Benchmark Database of Barrier Heights for Heavy Atom Transfer, Nucleophilic Substitution, Association, and Unimolecular Reactions and Its Use to Test Theoretical Methods. *J. Phys. Chem. A* **2005**, *109*, 2012−2018.

(111) Štrajbl, M.; Sham, Y. Y.; Villà, J.; Chu, Z.-T.; Warshel, A. Calculations of Activation Entropies of Chemical Reactions in Solution. *J. Phys. Chem. B* **2000**, *104*, 4578−4584.

(112) Villà, J.; Štrajbi, M.; Glennon, T. M.; Sham, Y. Y.; Chu, Z. T.; Warshel, A. How important are entropic contributions to enzyme catalysis. *Proc. Natl. Acad. Sci. U.S.A.* **2000**, *97*, 11899−11904.

(113) Štrajbl, M.; Florián, J.; Warshel, A. Ab Initio Evaluation of the Potential Surface for General Base-Catalyzed Methanolysis of Formamide: A Reference Solution Reaction for Studies of Serine Proteases. *J. Am. Chem. Soc.* **2000**, *122*, 5354−5366.

(114) Štrajbl, M.; Florián, J.; Warshel, A. Ab Initio Evaluation of the Free Energy Surfaces for the General Base/Acid-Catalyzed Thiolysis of Formamide and the Hydrolysis of Methyl Thiolformate: A Reference Solution Reaction for Studies of Cysteine Proteases. *J. Phys. Chem. B* **2001**, *105*, 4471−4484.

(115) Torrie, G. M.; Valleau, J. P. Nonphysical sampling distributions in Monte Carlo free energy estimation: Umbrella sampling. *J. Comput. Phys.* **1977**, *23*, 187−199.

(116) Kumar, S.; Bouzida, D.; Swendsen, R.; Kollman, P.; Rosenberg, J. The weighted histogram analysis method for free energy calculations on biomolecules 1: The method. *J. Comput. Chem.* **1992**, *13*, 1011−1021.